Journal of Iberian Geology
https://doi.org/10.1007/s41513-020-00147-8

RESEARCH PAPER

Ordovician volcanic rocks record rifting, Variscan metamorphism and gold mineralization processes (Truchas Syncline, NW Iberia, Spain)

L. González-Menéndez[1] · F. Gómez-Fernández[2] · J. K. Cunningham[3] · S. Menéndez[4] · P. Caldevilla[2] · G. Gallastegui[5] · A. Cuesta[6]

Received: 2 July 2020 / Accepted: 27 October 2020

Abstract

Ordovician volcanic rocks outcrop in several locations of the NW Iberian Variscan belt. Their composition is mainly basaltic (with less acid types) and occur as volcanic-volcanoclastic layers within a shale-slate succession. This work focuses on volcanic and related rocks within a prominent Variscan structure, the Truchas Syncline. We studied field relations, petrography, mineralogy, geochemistry and conducted thermodynamic modelling to review the petrogenesis and establish the evolution of these volcanic rocks classified as within-plate alkaline basalts (high Ti/Y, Nb/Y and Nb/Yb). Crustal contamination is absent given the elevated Nb/La ratio (1–1.5). These features indicate low melting degrees of the upper mantle and a continental rifting environment. The finding of Ordovician orthid brachiopods in some of the volcanoclastic rocks suggests a shallow marine environment for the volcanic deposition. Variscan metamorphism occurred at lower greenschist conditions with chlorite-temperatures of 374 ± 6 °C. Quartz + carbonate veins indicate that H_2O–CO_2 metamorphic fluids traversed some volcanic rocks, reacting with Ca–Fe–Mg phases to produce carbonates (Mg-calcite–Fe-dolomite). For this event, T-XCO_2 modelling indicates temperatures below 350–360 °C and fluid XCO_2 between 0.10 and 0.45. Such fluids can be important carriers of Au and might explain gold deposits in adjacent quartzites. Metasomatic shales (Fe-chlorite + quartz) outcrop nearby and were derived from a mixed protholith of shales and minor volcanic components. Its geochemistry shows Fe enrichment and high peraluminosity. Variscan deformation further modified its geochemistry causing Si-depletions and relative increases of other elements (K, Na, Ti, Al, Rb, Sr, Ba and LREE) in shear zones domains.

Keywords Volcanic rocks · Metamorphism · Ordovician · Variscan · Truchas Syncline · Luarca formation

Resumen

Rocas volcánicas Ordovícicas afloran en el Macizo Varisco del noroeste de la Península Ibérica. Su composición es basáltica (con escasos términos ácidos) y forman niveles volcánicos y volcanoclásticos dentro de una sucesión de pizarras Ordovícicas. En este trabajo se estudian estas rocas en el Sinclinal de Truchas, una importante estructura Varisca. Se investigan las relaciones de campo, petrografía, mineralogía, geoquímica y se realiza un modelo termodinámico para revisar la petrogénesis de estas rocas volcánicas clasificadas como basaltos alcalinos intra-placa con elevadas relaciones de Ti/Y, Nb/Y y Nb/Yb. No se observan indicios de contaminación cortical, dadas las elevadas relaciones de Nb/La observadas (1–1.5). Esta geoquímica indica bajos grados de fusión del manto superior y un ambiente tectónico de rifting continental. La presencia de restos de braquiópodos órtidos del Ordovícico en algunas rocas volcanoclásticas sugiere un ambiente marino poco profundo para su depósito. El metamorfismo varisco se produjo en condiciones de esquistos verdes con temperaturas de clorita de 374 ± 6 °C.

✉ L. González-Menéndez
l.gonzalez@igme.es

[1] IGME: Unidad de León, Avda.Real 1. Parque Científico, 24006 León, Spain

[2] Área de Prospección E Investigación Minera, E.S.T.I. Minas, Universidad de León, 24007 León, Spain

[3] Dpt. Earth and Planetary Sciences, Birkbeck College, University of London, Malet Street, London WC1E 7HX, UK

[4] IGME: Museo Geominero, Ríos Rosas 23, 28003 Madrid, Spain

[5] IGME: Unidad de Oviedo, Matemático Pedrayes 25, 33005 Oviedo, Spain

[6] Departamento de Geología, Universidad de Oviedo, 33005 Oviedo, Spain

Diversas venas de cuarzo y carbonatos observadas representan fluidos metamórficos de H_2O–CO_2 que atravesaron algunas rocas volcánicas, reaccionando sus minerales de Ca–Fe–Mg para producir carbonatos (Mg-calcita–Fe-dolomita). Para este evento, el modelo de T-XCO_2 realizado indica temperaturas por debajo de 350–360 °C y XCO_2 del fluido entre 0.10 y 0.45. Estos fluidos pueden ser portadores de oro en solución y podrían explicar mineralizaciones descritas en las cuarcitas adyacentes. Varios niveles de pizarras metasomáticas (formadas por clorita rica en hierro y cuarzo) afloran en zonas próximas. Derivan de un protolito mixto de pizarras y componentes volcánicos menores. Su geoquímica muestra enriquecimiento en hierro y elevada peraluminosidad. La deformación varisca modificó adicionalmente su geoquímica causando empobrecimientos de sílice e incrementos relativos de otros elementos en zonas de cizalla (K, Na, Ti, Al, Rb, Sr, Ba y LREE).

Palabras Clave Rocas volcánicas · Metamorfismo · Ordovícico · Varisco · Sinclinal de Truchas · Formación Luarca

1 Introduction

AQ1 Ancient volcanic and volcanoclastic rocks are important in earth science research because they can contain a rich record of past geological conditions: the nature of their mantle/crustal sources and the composition of the crust traversed if contamination processes happened. Even crustal and lithospheric thicknesses estimations are possible from the study of volcanic rocks (Liu et al. 2016 and references therein). Furthermore, they record the type of emplacement conditions, possible contact metamorphism effects, surficial environmental conditions and type of alteration processes. Volcanic rocks of basic to intermediate composition are particularly susceptible to metamorphic and hydrothermal processes affecting their geological surroundings (Bucher and Grapes 2011).Their ages can also be calculated by different radiometric methods (K–Ar, Ar–Ar, Sm–Nd) provided alteration has not been very intense.

Lower Paleozoic volcanic (±volcanoclastic) rocks in the NW Iberian Variscan belt have been studied to infer the nature of the mantle source and emplacement conditions prior the Variscan orogenic event (Valverde-Vaquero 1992; Gallastegui et al. 1992; Suárez et al. 1993; Villa et al. 2004; Brendan Murphy et al. 2008 among others). These volcanic rocks occur in different geological domains of NW Spain and usually record their emplacement conditions and subsequent evolution through alteration, metasomatism, Variscan metamorphism-deformation and gold mineralization in nearby host rocks (Villa et al. 2004).

The Variscan Truchas syncline (Fig. 1; Suárez et al. 1994; Fernández-Lozano, 2012; Rodríguez Fernández et al. 2015) is a prominent Carboniferous structure located in the northern part of the Central Iberian Zone (CIZ). It is composed of lower Paleozoic shale-sandstone-quartzite successions affected by folds, foliations and a low metamorphic grade (greenschists) attained during the Variscan orogenic event (≈ 320–350 Ma). Mafic ± felsic volcanic and volcanoclastic rocks of Ordovician age occur as sills and layers within the shale formations. Furthermore, late Variscan gold mineralization appear in quartz veins near the contact between Ordovician volcanic rocks, shales and quartzites (Gómez-Fernández et al. 2012).

The present work focuses on the field relations, fossil occurrences, petrography, mineralogy and geochemistry of the SE Truchas syncline volcanic and related rocks. Our aim is to understand its origin, emplacement environment, hydrothermal alteration, metamorphism, metasomatism, deformation and possible relations with nearby gold mineralization. All these processes have played a role in configuring the current features in these rocks, causing in some cases, deviations from the expected whole rock composition (González-Menéndez et al. 2019). This study reinforces the rifting hypothesis for the origin of the studied basaltic volcanic rocks. Some of them are interpreted as metasomatic, derived from shales ± sandstones, mixed with a minor volcanic component and affected by Fe-metasomatism and SiO_2-depletion processes. H_2O–CO_2 late-stage fluids (post-peak metamorphic), known to be candidates for gold transport in orogenic settings (Kesler 2005; Yardley and Bodnar 2014), left a key record in the form of carbonation of some of the mafic volcanic rocks studied.

2 Geological background and sampling site description

The Truchas syncline region has a very complete and representative record of Ordovician sedimentary rocks (shales, sandstones, quartzites, ± limestones) including abundant volcanic and volcanoclastic rocks. The basal part of the Truchas syncline is formed by the Ollo de Sapo metavolcanic orthogneiss (Fig. 2) (Díez Montes 2007), cropping out to the south and to the east of the studied zone (Fig. 1). The overlying sedimentary formations are: Capas de los Montes (Lower Ordovician quartzites, microconglomerates, black shales and sandstones), Cuarcita Armoricana (quartzites, Lower to Middle Ordovician), Capas de Transición (shales and sandy shales), Luarca Formation (Middle Ordovician black shales-slates), interlayered mafic/felsic metavolcanic rocks, the Casaio Formation (Upper Ordovician quartzites,

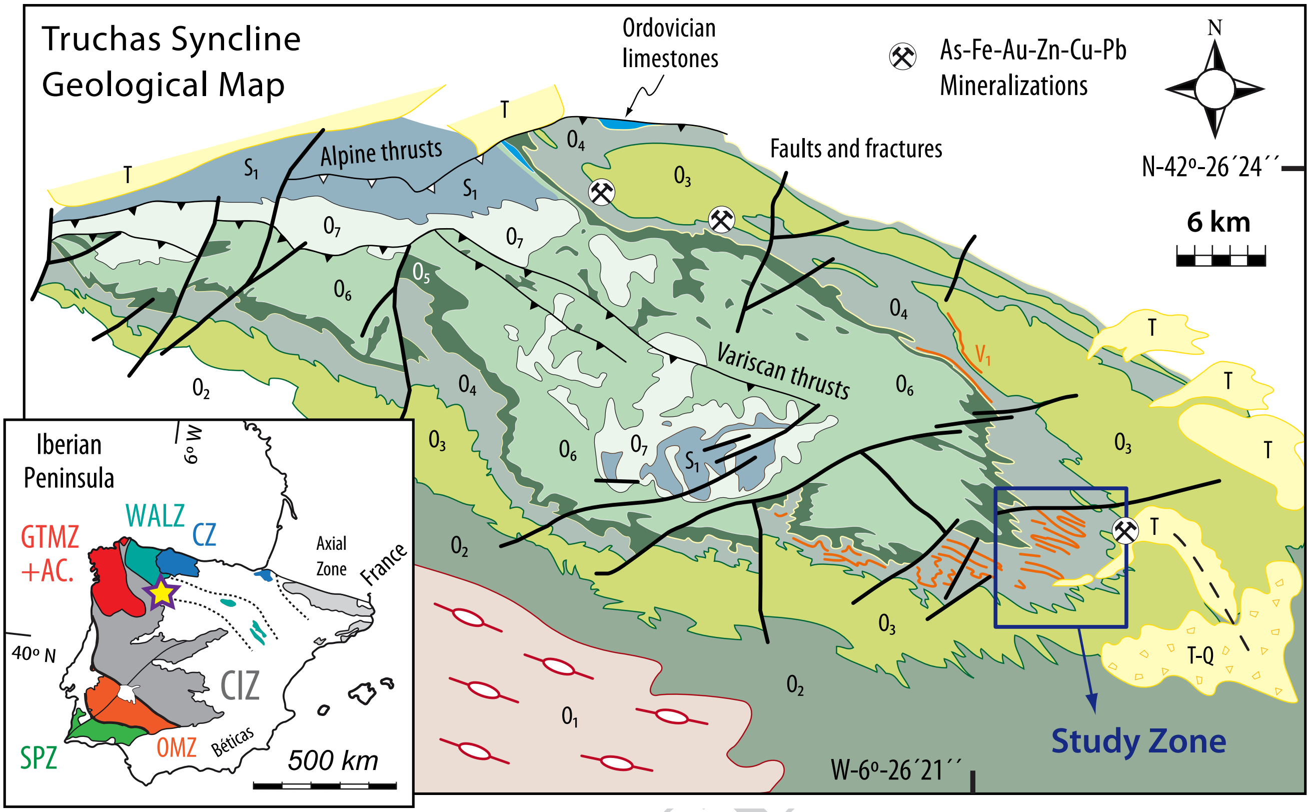

Fig. 1 Geological map of the Truchas Syncline region, NW Spain (modified after Suárez et al. 1994). *O1* Ollo de Sapo orthogneisses, *O2* Capas de los Montes Formation: schists, quartzites and sandstones, *O3* Cuarcita Armoricana and Capas de Transición formations, *O4* Luarca Formation, shales-slates, *V1* volcanic and volcanoclastics layers and sills, *O5* Casaio Formation, shales ± quartzites, *O6* Rozadais Formation, shales, *O7* Losadilla Formation, shales ± sandstones. *S1* Llagarinos Formation, ampelitic shales, *T* Tertiary, conglomerates and sands, *CZ* Cantabrian Zone, *WALZ* West Asturian-Leonese Zone, *GTMZ* Galicia-Trás-os-Montes Zone, *CIZ* Central Iberian Zone, *OMZ* Ossa Morena Zone, *SPZ* South Portuguese Zone

shales and rare carbonate beds), the Rozadais Formation (Upper Ordovician shales), the Losadilla Formation (Upper Ordovician shales and sandstones) and the Llagarinos Formation (Silurian ampelitic black shales ± sandstones).

The volcanic rocks are interlayered with shales (Luarca Fm) and were described in the geological maps of this area (Suárez et al. 1994; Villar Alonso et al. 2019 and references therein). The shales have been attributed to a Middle Ordovician age by paleontological studies by Gutiérrez et al. (1999; 2002). Regarding the volcanic rocks, petrological-geochemical studies of these and other outcrops from the Central-Iberian Zone (CIZ), the West-Asturian Leonese Zone (WALZ) and the Cantabrian Zone (CZ) have been done by different authors (Valverde-Vaquero 1992; Gallastegui et al. 1992; Suárez et al. 1993; Villa et al. 2004; Brendan Murphy et al. 2008). These studies suggest a crustal origin for the felsic types, an enriched mantle source for the mafic ones and an intraplate rifting environment for the intrusion and emplacement of all these volcanic rocks.

The geodynamic setting for the Ordovician sedimentation and the felsic magmatism in central and NW Iberia has been discussed by Díez Montes 2007 and references therein. Valverde-Vaquero and Dunning (2000) proposed a back-arc setting to explain the felsic magmatism and volcanism represented by the Ollo de Sapo formation. Recent interpretations propose different hypotheses: an environment evolving from a compressive geodynamic setting to a passive one (Villaseca et al. 2016) vs. a purely extensional regime (Montero et al. 2017).

In the present work, we study and review the previous mapping of volcanic rocks at the southeast domain of the Truchas syncline (Fig. 3). The volcanic layers were affected by recumbent/inclined, meter-scale folds, apparently south vergent but coherent with the main fold geometry of the Truchas syncline (Suárez et al. 1994; Rodríguez Fernández et al. 2015). Some of the volcanoclastic rocks preserve a stratification (Fig. 4a) that records volcanoclastic deposition. In some outcrops, scoriaceous layers bordering the main volcanic masses appears (Fig. 4b, c) attesting to the presence of lava bodies, deposited above the shales, and cooling rapidly in their upper borders (samples C-1B, CF-2, and M3 in Fig. 3). Samples IGS-39 and IGS-40 are volcanic rocks located 2 km

Journal : Large 41513 | Article No : 147 | Pages : 23 | MS Code : 147 | Dispatch : 9-11-2020

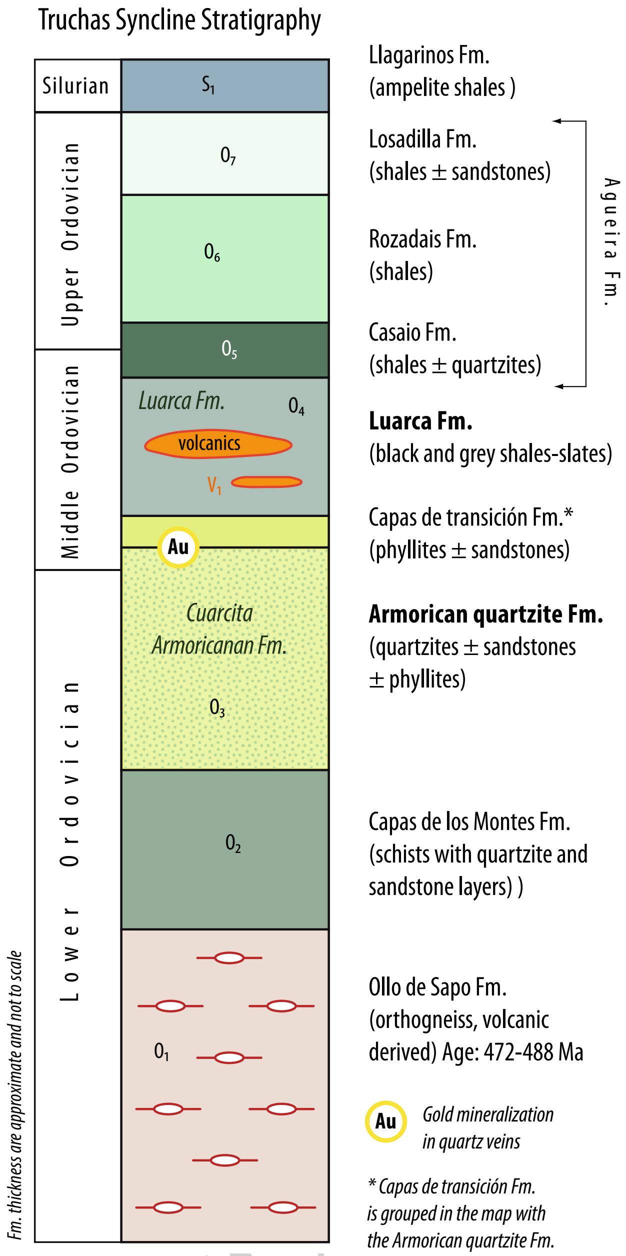

Fig. 2 Simplified stratigraphy of the Truchas Syncline region, NW Spain (modified after Suárez et al. 1994). The Upper Ordovician formations, Casaio, Rozadais and Losadilla, formed by shales ± sandstones, are grouped in other northern geological settings, into the Agüeira Formation

to the south of the study zone. Other sets of rocks have a more difficult assignment having no clear volcanic features, lacking top scoriaceous layers and showing a high foliation density in their contacts with the shales (samples CF-3, C-5, C-5R, C-6, C-6RA, C-6RB and C-7 in Fig. 3). We named these rocks metasomatic shales due to significant geochemical differences when compared to volcanic or volcanoclastic rocks and having more affinity with shale/slate compositions (Ward and Gómez-Fernández 2003; Gómez-Fernández et al. 2009).

3 Fossil occurrences in the volcanoclastic rocks

The existence of a diverse fossil record in the Luarca Formation (equinoderms, bryozoans, bivalves, rostroconchs, cephalopods, gastropods, brachiopods, ostracods, hyolithids, graptolites and trilobites) has been observed in northwestern Spain (CIZ, WALZ and CZ) where these materials extensively outcrop (Gutiérrez-Marco et al. 1999 and references therein). Nevertheless, the presence of fossil fauna within the volcanoclastic levels interlayered in the Luarca Formation is scarce. Pérez-Estaún (1974; 1978) was the first who reported the occurrence of *Redonia* sp. (shells of bivalves determined by prof. C. Babin) in volcanoclastic layers close to the base of the Luarca Formation (Valdavido, southern Truchas Syncline). Matas and Velando (1982) also reported the presence of *Redonia* in the volcanoclastic levels of the studied area at northern Cunas. *Redonia* findings allowed assigning an Ordovician age to these levels, with no further precisions. Subsequently, Babin and Gutiérrez-Marco (1991) reassigned as *Redoniades hayesi* the previous *Redonia* sp. bivalves. New fossil material, *Tolmachovia* n. sp. and *Porambonites?* sp., were described from the first volcanoclastic levels referenced (Gutiérrez-Marco et al. 1999) and an accurately age was established: Oretanian.

In the Real syncline (Mondoñedo Nappe, WALZ) there are also thin volcanic intercalations at the base of Luarca Shales Formation where Marcos et al. (1980) cited fragments of indeterminate shells. Emig and Gutiérrez-Marco (1997) assigned these fossils to linguliids bivalves concentrated in a single horizon.

At the Cabo Peñas and Cabo Vidrias (CZ) volcanoclastic rocks interlayered with sandstones, shales and slates, form the lower Sect. (400 m thick) of the of the Castro Formation that conformably overlies the Luarca Formation. The fossil record here is composed of *Mecwanella vulcanica*, *Hesperinia asturica*, *Ectillaenusgiganteus*, *Pinaceocladichnus bulbosus, Ogmoopsis?* sp., Asaphina gen. indet., Bryozoa gen. indet. and Pelmatozoa gen. indet. These levels have been reassigned as late Dobrotivian age (Villas et al. 1989; Gutiérrez-Marco et al. 1999). Paleoenvironmental conditions related to these volcanoclastic horizons indicate calm and locally warm water around the volcanic emission sites, episodically colonized by opportunistic communities of bryozoans, echinoderms and brachiopods (Gutiérrez-Marco et al. 1999).

A new fossil record is reported here from the studied area. Volcanoclastic rocks of Cunas C-4 site (Fig. 3) preserve outer molds of orthid brachiopod valves (Fig. 4d).

Journal : Large 41513	Article No : 147	Pages : 23	MS Code : 147	Dispatch : 9-11-2020

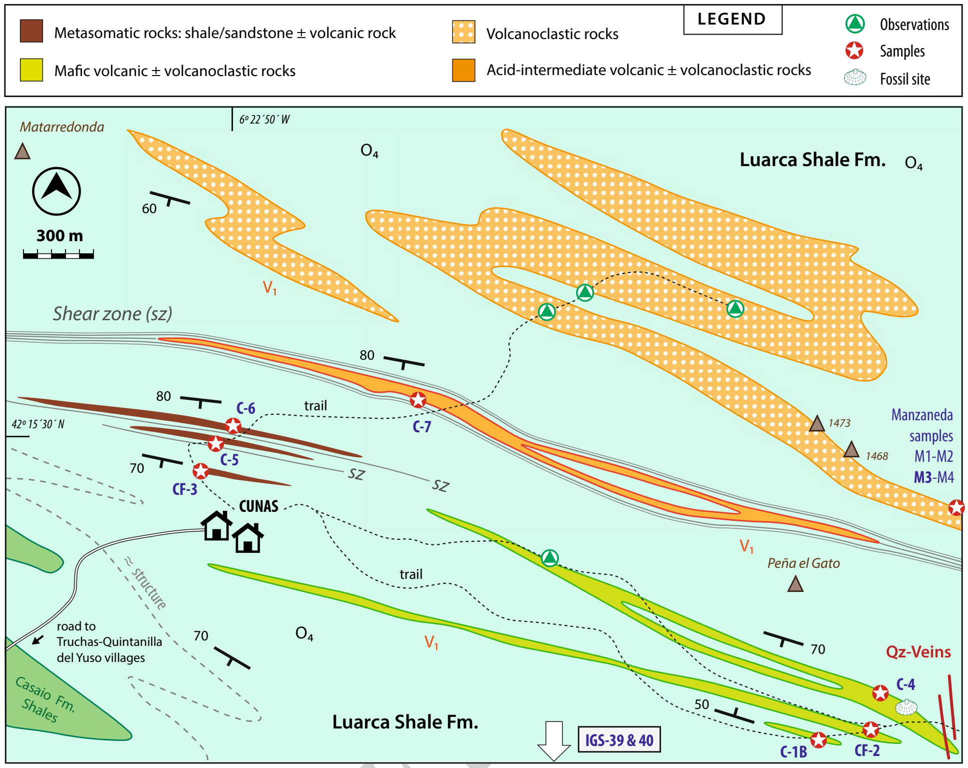

Fig. 3 Geological map of the studied zone (modified after Suárez et al. 1994; Villar Alonso et al. 2019). Sampling is shown with the symbol stars. Locations C-5 and C-6 include sets of samples in order to record the variation in foliation intensity (C-5: C-5, C-5R; C-6: C-6, C-6RA, C-6RB). Bold numbers correspond to samples were EMPA and/or bulk rock analyses was performed

Unfortunately, the preservation of samples is very poor for an accurate taxonomical determination. They have been collected to be housed in Geominero Museum under the numbers from MGM-8152O to MGM-8160O. Valves, both dorsal and ventral, are disarticulated; most of them show no evidence of sorting or preferred orientation. They have not suffered significant breakage and therefore did not suffer considerable transportation. Conversely, the emission of volcanic materials implies a very high ambient temperature and survival in the site emission probably was not possible. Thus, the depositional ambient could have been a low-energy media with fine-medium sand and small size basalt debris supplied by nearby volcanic eruptions. Villas et al. (1989) suggest that a low rate of sedimentation and long periods before burial, subsequent to death, enhanced the disarticulation of shells and infestation by borers. These conditions could have been similar in the studied area. This is supported by the occurrence of *Redonia deshayesi* and *Tolmachovia* sp. in these volcanoclastic levels. They are usually infaunal filter feeders but some specimens of spanish *Redonia deshayesi* show a bryozoan incrustation, suggesting that a part of the shell projected above the seabed (Polechová 2016) which normally requires a low rate of sedimentation. *Tolmachovia* environment conditions are interpreted to be quiet and sublittoral marine platform (Gutiérrez-Marco 1997).

4 Methods

Field geology and sampling was conducted in the south-eastern part of the syncline where an important outcrop area of volcanic rocks is mapped in the region. Samples were taken from different volcanic/volcanoclastic units in large enough amounts (5–10 kg) to ensure chemical and mineralogical homogeneity of the rock samples. Thin sections were made for each sample for petrography studies under the optical microscope, SEM (scanning electronic microscope) and EMPA (electron micro-probe analysis) investigations. SEM was done at Leon University (Spain) using a JEOL JSM-6480 scanning electron microscope equipped with an Oxford D6679 EDS detector. EMPA was done at Oviedo University (Spain) using a Cameca SX-100 electron microprobe operated at 15 keV accelerating voltage, 15 nA beam current and and 2 µm beam size. Orthoclase (Si), wollastonite (Ca), MnTi (Ti, Mn), magnetite (Fe), albite (Na), Al_2O_3 modified (Al), cromite (Cr), NiO (Ni), MgO (Mg) and apatite (P) were used as standards for determination of the respective elements in brackets. Most of the bulk rock analysis was performed by ICP-AES (Inductively Coupled Atomic Emission Spectroscopy) for major elements and ICP-MS (Inductively Coupled

Journal : Large 41513 | Article No : 147 | Pages : 23 | MS Code : 147 | Dispatch : 9-11-2020

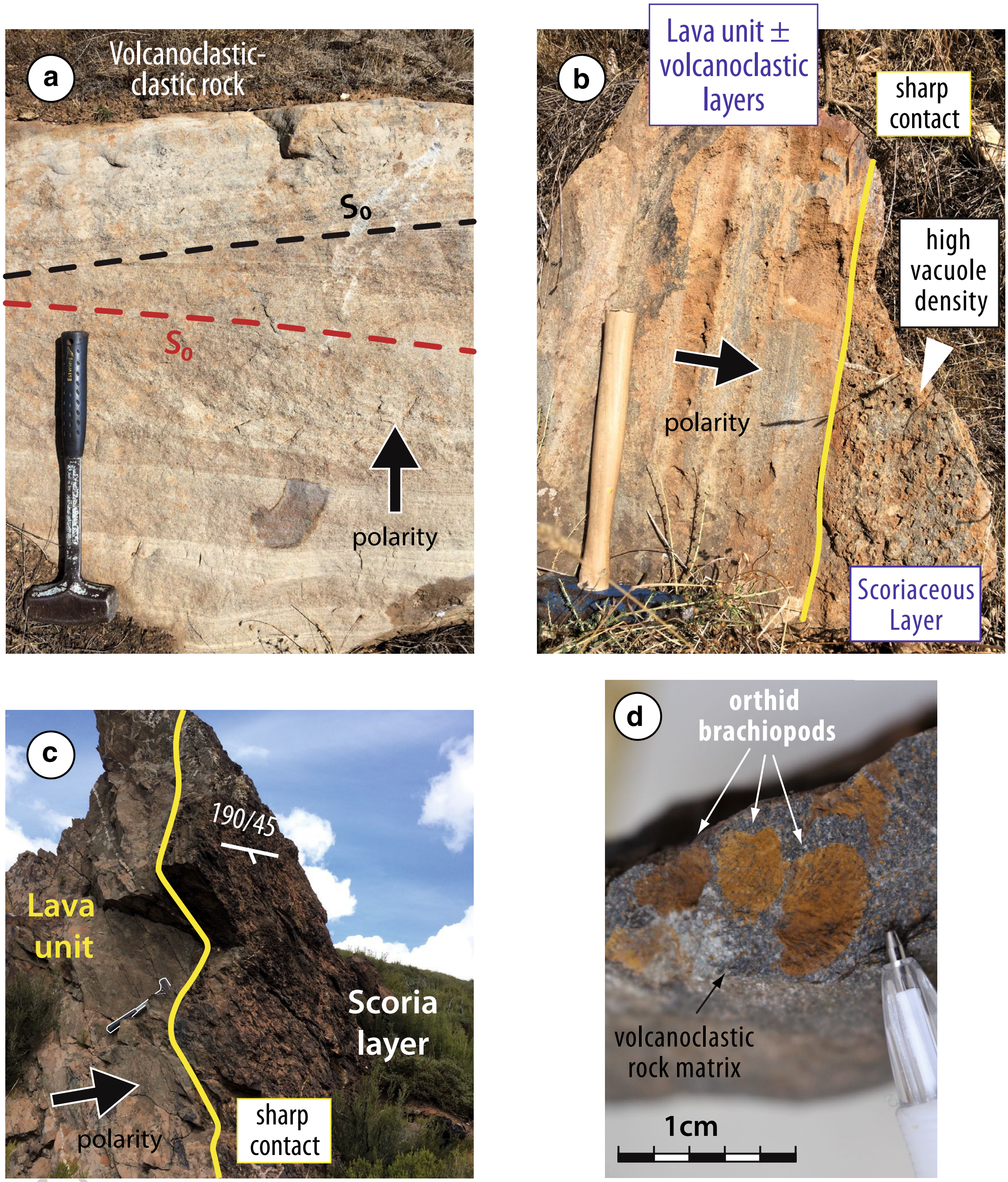

Fig. 4 Field relations of the studied volcanic/volcanoclastic rocks. **a** Cross bedding in a mixed volcanic-sandstone rock. **b** Scoriaceous layer developed in the border of a volcanic rock. **c** Volcanic rock interpreted as a lava flow shielded in its upper border by a scoria layer. **d** Shell molds of Ordovician orthid brachiopods within a volcanoclastic layer (C-4 in Fig. 3.)

Mass Spectrometry) for trace and rare earth elements. The analyses were carried out at the ALS Global laboratory in Ireland (ME-ICP06 and ME-MS81 procedures). A simplified summary of these methods is given below. For the major oxides, a milled sample (0.1 g; < 0.05 mm grain size) is added to lithium metaborate (35.3%)/lithium tetraborate (64.7%) flux, mixed well and fused in a furnace at 1000 °C. The resulting melt is then cooled and dissolved in 100 ml of 4% nitric acid + 2% hydrochloric acid. This solution is then analyzed by ICP-AES and the results are corrected for spectral inter-element interferences. For the trace and rare earth elements, a milled sample (0.1 g; < 0.05 mm grain size) is added to lithium metaborate (35.3%) / lithium tetraborate (64.7%) flux, mixed well and fused in a furnace at 1025 °C. The resulting melt is then cooled and dissolved in an acid mixture containing nitric,

Journal : Large 41513 | Article No : 147 | Pages : 23 | MS Code : 147 | Dispatch : 9-11-2020

hydrochloric and hydrofluoric acids. This solution is then analyzed by inductively coupled plasma–mass spectrometry. Samples IGS-39 and IGS-40 were taken and analyzed during a previous and unpublished geological study in the region by one of the authors (G. Gallastegui). Major and some trace elements of these samples were analyzed by XRF at the Technical-Scientific Services of Oviedo University (Spain) using a WD-XRF spectrometer (model 2404; PANalytical) coupled with a Rh tube. Major element analyses were performed using glass beads of powdered rocks after fusion with lithium tetraborate. Precision of the XRF technique was better than ± 1% relative. Trace elements were determined on pressed pellets with Elvacite. Raw data were processed using Pro-Trace-XRF PANalytical software. Other trace elements (Cs, Ga, Hf, Ta, Li, Sc) and rare earth elements (REE) were analyzed by ICP-MS following sample decomposition with lithium metaborate at the Geochronology and Geochemistry-SGIker facility of El País Vasco University/EHU (Spain) (see García de Madinabeitia et al. 2008 for additional details). All the results are shown in Tables 1, 2 and 3.

5 Petrography and mineralogy

5.1 Volcanic and volcanoclastic rocks

The volcanic and volcanoclastic rocks are characterized by the presence of plagioclase crystals, volcanic fragments and scoriaceous margins at the top of the volcanic layers. The main petrographic features are the micro-porphyritic textures, phenocrysts of plagioclase, absence of any other primary phases and presence of secondary minerals such as K-feldspar, quartz, sericite and widespread chlorite. By these criteria, samples C-1B, CF-2, C-4, C-7, M1, M2A, M3 and M4 (Fig. 3) are classified as volcanic and volcanoclastic.

The volcanic rocks (C-1B, CF-2,C-4, M3) are composed of plagioclase phenocrysts (Fig. 5a) and some rock fragments within a matrix of plagioclase + chlorite ± quartz ± K-feldspar ± sericite. Rare prehnite crystals were observed in two samples. Carbonate minerals and chlorite are abundant in some rocks and scarce in others. Carbonates replace plagioclase phenocrysts, Ca–Fe–Mg phases and rock fragments (Fig. 5b). Growth of carbonate over chlorite is observed. Quartz + carbonate and pure carbonate veins

Table 1 Chlorite analyses by EMP. Oxide contents are in wt.%. Volc.: volcanic rock

Refs.	m3a n = 1	m3b n = 1	m3c n = 1	m3d n = 1	m3e n = 1	m3f n = 1	m3g n = 1	m3h n = 1	m3i n = 1	m3j n = 1	Pomb Avg n = 12	Llamas Avg n = 8
Rock	Volc	Volc	Volc	Volc	Volc	Volc	Volc	Volc	Volc	Volc	Slates	Slates
SiO_2	25.448	25.779	26.574	25.816	25.947	25.553	25.848	25.979	25.425	26.246	23.71	23.69
TiO_2	0.045	0.008	0.010	0.108	0.028	0.024	0.028	0.055	0.045	0.035	0.026	0.023
Al_2O_3	23.467	23.967	24.401	23.806	23.985	23.797	24.092	24.042	23.498	23.728	21.19	21.15
FeO	19.737	19.668	19.850	19.885	19.902	19.793	20.035	19.859	19.891	20.126	36.66	36.71
MnO	0.107	0.058	0.066	0.088	0.058	0.036	0.028	0.052	0.031	0.017	0.45	0.43
MgO	17.008	17.339	16.611	16.997	16.898	17.212	17.007	16.491	16.285	16.925	6.03	6.04
CaO	0.071	0.051	0.062	0.076	0.046	0.062	0.045	0.068	0.098	0.085	0.027	0.030
Na_2O	0.009	0.028	0.000	0.056	0.035	0.000	0.000	0.030	0.000	0.002	0.012	0.014
Total	86.332	87.330	88.091	87.145	87.386	86.900	87.376	86.968	85.769	87.498	88.22	88.25
T °C	377.846	379.328	363.358	376.228	373.942	382.503	378.137	370.108	375.220	366.444	385.33	385.34
Refs.	C3a n = 1	C3b n = 1	C3c n = 1	C3d n = 1	C3e n = 1	C3f n = 1	C3g n = 1	C3h n = 1	C3i n = 1	C3j n = 1	C3k n = 1	C3l n = 1
Rock	Met	Met	Met	Met	Met	Met	Met	Met	Met	Met	Met	Met
SiO_2	24.069	21.952	22.934	23.164	22.759	23.303	22.719	23.589	23.189	22.224	22.544	22.478
TiO_2	0.039	2.598	0.033	0.068	0.004	0.074	0.030	0.017	0.035	0.056	0.000	0.133
Al_2O_3	24.171	23.207	23.819	22.719	23.389	23.833	23.798	23.764	23.321	23.662	23.925	23.681
FeO	34.543	35.157	35.743	36.477	35.812	36.635	36.467	34.974	36.427	36.754	36.389	35.473
MnO	0.067	0.109	0.083	0.130	0.071	0.083	0.079	0.078	0.120	0.141	0.116	0.082
CaO	0.017	0.032	0.039	0.031	0.008	0.018	0.033	0.033	0.021	0.025	0.002	0.015
Na_2O	0.027	0.027	0.000	0.046	0.000	0.000	0.000	0.019	0.035	0.008	0.000	0.011
Total	87.793	88.248	87.798	88.261	87.383	89.180	88.544	88.215	88.395	88.273	88.382	87.751
T °C	386.556	454.434	415.900	407.272	416.204	414.974	428.276	402.522	411.292	440.096	431.459	430.683

Met. metasomatic shale, *Pomb* Pombriego, *Avg* Average. *T °C* calculated by the method of Jowett 1991

Journal : Large 41513 | Article No : 147 | Pages : 23 | MS Code : 147 | Dispatch : 9-11-2020

Table 2 Carbonate analyses by EMP. Oxide contents are in wt.%. Volc.: volcanic rock

Ref	M3-1 n = 1	M3-2 n = 1	M3-3 n = 1	M3-4 n = 1	M3-5 n = 1	M3-6 n = 1	M3-7 n = 1	M3-8 n = 1	M3-9 n = 1	M3-10 n = 1
Rock	Volc	Volc	Volc	Volc	Volc	Volc	Volc	Volc	Volc	Volc
CaO	33.355	32.945	32.252	32.693	31.854	30.735	30.796	31.926	32.074	33.568
FeO	7.126	7.580	7.206	6.525	6.319	6.165	7.138	7.257	7.420	6.901
MgO	15.362	15.089	14.740	15.633	16.066	15.427	15.176	15.463	15.786	15.474
MnO	0.6731	0.6593	0.575	0.804	0.5129	0.6962	0.6272	0.6498	0.5252	0.8107
SiO_2	0.2373	0.0692	0.0986	0.3405	0.1482	0.0847	0.078	0.0268	0.0325	0.1366
Al_2O_3	0.1156	0.0501	0.0166	0.2359	0.0645	0.0751	0.0848	0.0299	0.0406	0.075
P_2O_5	0.2164	0.2427	0.2376	0.2631	0.2077	0.169	0.2503	0.2103	0.1857	0.2411
CO_2	42.531	43.087	44.756	43.297	44.599	46.422	45.692	44.075	43.833	42.582
Total	99.7034	99.962	99.978	99.971	99.8918	99.983	99.984	99.668	99.966	99.963

cut across the primary and secondary mineral assemblage in some samples (Figs. 5c & d). A SEM study of the M3 sample reveals that the carbonate phases are mainly Fe-bearing dolomite or Fe–Mg calcite, and the plagioclase phenocrysts are nearly pure albite (Na-rich). Apatite, rutile, chalcopyrite and sphalerite were identified. The textures are microporphyritic with a significant difference in size between phenocrysts and matrix. Some amygdales occur, filled with growing crystals of quartz + feldspar, and iron oxides in the center. Slight mineral orientation/rock deformation is observed in some of the samples.

The volcanoclastic rocks (C-4, M1, M2A, M2C, M4, C-7) are composed of different volcanic fragments with similar mineralogy as the volcanic rocks: plagioclase laths in a chlorite ± quartz matrix. Accessory phases include sericite, muscovite, tourmaline, iron sulphides, and zircon. Occasionally outsized plagioclase ± quartz crystals appear. The different fragments have rounded/elliptical and lobule shapes defining a broad oriented pattern. These fragments have thin and sharp dark borders composed of iron oxides. No preferred mineral grain orientations were observed. C-7 sample is more felsic and its texture is dominated by a high foliation density.

5.2 Metasomatic shales

The metasomatic rocks were originally mapped as volcanic, but this affinity was dubious because they lack the field criteria previously defined. These are the samples: CF-3, C-5, C-5R, C-6, C-6RA and C-6RB (Fig. 3). Sample CF-3 has been studied with more detail (Fig. 5e,f). It is composed of quartz (≈ 40–45%) ± rock fragments (quartz rich, pelitic or limolitic) and a chlorite matrix (≈ 45–50%) that surrounds most of the other mineral phases. Minor patches of sericite also occur. Neither feldspars (plagioclase/K-feldspar) nor carbonate phases are present. The rock has a subtle subsolidus orientation defined by the chlorite matrix. Quartz is not internally deformed but some crystals have their long axis approximately parallel to the chlorite fabric. This might indicate that the deformation was mainly transferred to the more ductile chlorite matrix. A SEM study of this rock reveals that the chlorite is Fe-rich (chamosite) and the most common accessory minerals are zircon, rutile and xenotime. Samples C-5 and C-6 series are similar to CF-3, though their texture is defined by a strong foliation defined by the oriented chlorite. Foliation density changes from very high strain, at the contact with the shales, to low strain away from this contact.

6 Chlorite temperatures and carbonate chemistry

Chlorite is a common secondary phase appearing in all the studied rocks. In the volcanic/volcanoclastic rocks it is probably replacing Fe–Mg bearing primary minerals such as pyroxenes or amphiboles that have been completely altered. We have analyzed some of these chlorites to characterize their chemistry and to estimate their temperatures of formation. Table 1 shows the chlorite compositions (measured by EMPA) and their crystallization temperatures calculated with the method described by Jowett (1991). The correlation of between T °C and the Al^4 corrected term is R = 0.981. Standard deviations estimated on specific studies was between 32 and 37 °C (Jowett 1991). Chlorites from the mafic volcanic-volcanoclastic rocks are classified as Mg-chlorites. They lie in the field of clinochlore in the diagram of Zane and Weiss (1998) (Fig. 6a) and have moderate to elevated Al contents (2.85–2.90 a.f.u.). Their calculated temperatures range from 363 to 382 °C and show a mean of 374 ± 6 °C (Fig. 6b). These temperatures are very similar to those calculated for chlorites in the Ordovician host shales (Pombriego and Llamas, Fig. 6b). Chlorites occurring in the metasomatic shales and shales are classified as Fe-chlorites (Fig. 6a). Their Al content is relatively high in the metasomatic shales (3–3.14 a.f.u.) and lower in the

Table 3 Bulk-rock analyses (ICP-AES, XRF, ICP-MS) of the studied samples

Ref	C-5	C-5R	C-6	C-6RA	C6-RB	CF-3	C-7	CF-2	C1B	IGS39	IGS40	Avg slates
Mode	Layer	Layer	Layer	Layer	Layer	Layer	Layer/Sill	Layer	Layer	Layer/Sill	Layer/Sill	Host Fm
Type	Met	Met	Met	Met	Met	Met	Volc_F	Volc	Volc	Volc	Volc	n = 10 / 6
SiO_2	33.9	50.6	43.5	58.1	40.5	54.8	74.5	42.9	43.8	39.43	44.89	52.93
TiO_2	2.01	0.99	1.19	0.7	1.45	0.76	0.44	2.48	2.06	1.96	1.84	1.04
Al_2O_3	21.3	17.6	17	12.6	23.8	11.75	13.85	18.2	14.8	12.43	12.35	23.33
FeO	32.7	20.4	27.8	21	21.5	23.5	5.17	11.4	11.1	11.09	10.45	9.36
MnO	0.09	0.08	0.1	0.07	0.06	0.11	0.02	0.16	0.15	0.17	0.12	0.08
MgO	3.02	2.43	3.62	2.65	2.71	2.58	0.82	6.76	7.37	8.65	10.63	2.53
CaO	0.23	0.08	0.7	0.27	0.33	0.12	0.1	4.48	5.94	7.3	2.07	0.36
Na_2O	0.2	0.36	0.04	0.05	0.53	0.03	0.47	5.33	4.43	3.72	4.08	1.22
K_2O	0.63	1.43	0.16	0.26	2.62	0.05	2.47	0.19	0.04	0.05	0.07	3.74
P_2O_5	0.44	0.25	0.61	0.3	0.37	0.26	0.14	0.7	0.29	0.26	0.19	0.21
A/CNK	14.9	7.7	11.24	14.74	5.52	36.52	3.81	1.06	0.81	0.63	1.17	3.50
Ba	121.5	359	36.2	65.9	644	22.5	397	373	67.1	23	57	707.83
Cr	130	60	150	50	90	60	50	110	150	343.22	575.44	105
Cs	1.53	3.03	0.5	0.62	4.81	0.26	4.16	0.56	0.13	0.23	0.30	8.19
Ga	24.6	21.9	22.2	17.2	29.4	17.1	20.2	23.4	18.7	18.54	18.57	27.25
Hf	7.3	5.2	4.5	4.1	6.5	4.1	5	5.2	4.1	3.50	3.22	4.72
Nb	46.7	38.1	35.2	27.9	35.2	33.2	38.6	54.9	41.6	27.94	26.27	19
Rb	28.4	65.5	6.9	12.1	122	2.7	113.5	6.8	0.4	0.59	8.00	161.83
Sr	62.4	101	33.1	24.3	171	16.2	142	303	494	365	186	157
Ta	2.6	3.2	1.6	2.3	2.5	2.2	3.2	2.5	2.2	1.78	1.55	1.35
Th	15.5	13.25	11.05	10.5	19.4	11.9	15.35	5.27	3.81	2.77	3.30	20.73
U	3.08	3.84	2.4	2.99	3.92	3.06	4.59	1.31	0.88	0.75	0.75	3.22
V	146	100	139	90	173	94	43	248	204	150	162	132
Y	45.7	45.9	50.1	36.8	47.9	41.1	40.6	26.8	17.8	16.25	15.59	39.82
Zr	225	165	151	126	202	125	167	227	170	130	119	162.33
Cu	41	2	17	6	4	8	2	25	6	46.56	105.06	36.33
Li	290	200	280	200	200	220	70	190	150	233.33	190.74	138.33
Ni	37	30	39	22	34	32	12	49	73	152.31	250.58	56
Pb	13	9	25	16	29	24	15	2	3	2.35	3.42	27
Sc	18	13	17	11	15	13	9	20	20	24	27	18.67
La	35.2	27.2	30.1	20.4	51.9	22.9	41.1	38.9	29.1	23.07	22.73	63.27
Ce	71.2	58.7	61	43.4	101.5	51.6	78.6	74.2	52.4	47.79	46.85	122.58
Pr	9.47	7.41	8.39	5.52	12.15	6.76	9.43	8.96	6.02	5.48	5.48	14.37
Nd	39.1	29.4	35.2	21.9	47.2	28.2	34.5	36	23.5	23.59	21.39	54.12
Sm	9.3	7.45	9.19	5.47	10.3	6.87	7.55	7.5	4.73	4.95	4.56	10.76
Eu	2.03	1.16	2.05	1.23	1.87	1.46	1.16	2.28	1.38	1.58	1.37	2.01
Gd	10.25	7.07	10.05	5.99	10.35	6.54	7.9	6.18	4.75	4.42	4.17	8.84
Tb	1.78	1.35	1.8	1.05	1.72	1.24	1.37	1.06	0.68	0.63	0.56	1.32
Dy	10.65	8.55	10.1	7.06	10.3	8.41	7.72	5.1	3.97	3.36	3.11	7.48
Ho	2.22	1.81	2.17	1.37	1.99	1.79	1.65	1.04	0.8	0.61	0.61	1.45
Er	6.12	5.16	6.13	4.01	5.48	5.36	4.45	3.19	1.98	1.57	1.54	4.08
Tm	0.97	0.78	0.98	0.64	0.76	0.78	0.63	0.38	0.26	0.23	0.22	0.58
Yb	5.91	4.82	6.09	4.12	4.73	5.39	3.78	2.71	1.79	1.53	1.44	3.69
Lu	0.86	0.68	0.91	0.61	0.68	0.75	0.59	0.32	0.26	0.23	0.22	0.55

Major elements in wt% and trace elements + REE in ppm

Volc: volcanic rock, *Met*. metasomatic shale, *Volc F* felsic volcanic rock

Journal : Large 41513 | Article No : 147 | Pages : 23 | MS Code : 147 | Dispatch : 9-11-2020

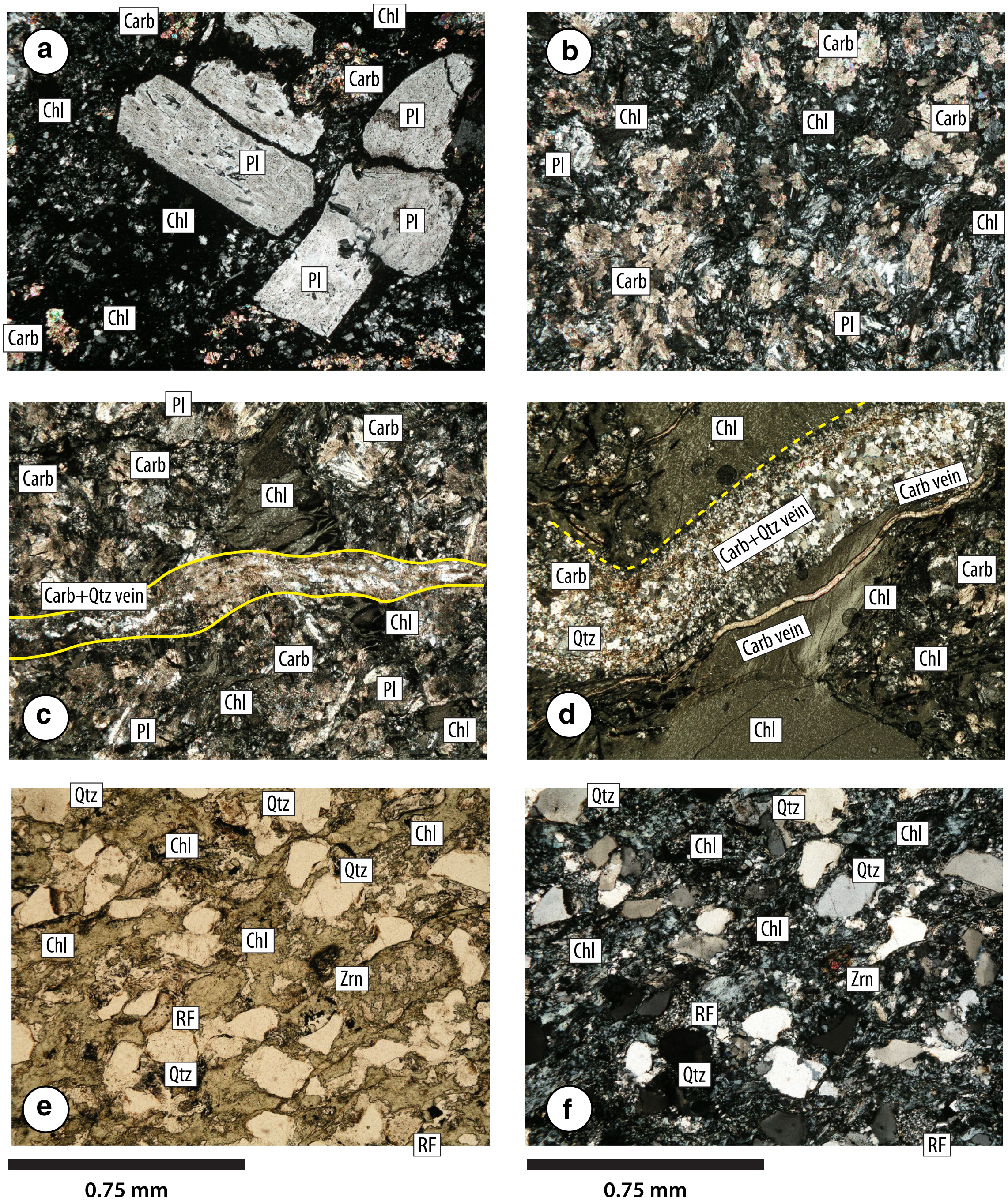

Fig. 5 Optical microscope images of the studied rocks. **a–d** The volcanic rocks (C-1B and CF-2) consist of plagioclase (Pl), chlorite (Chl) and variable amounts of carbonate phases. The carbonates grow over chlorite and plagioclase. Quartz + carbonate and carbonate veinlets cut across the chlorite phases (**c**, **d**). Metasomatic shales (**e**, **f**) consist of chlorite + quartz (≈ 50:45%) and other minor components such as rock fragments (RF) and accessory phases like zircon (Zrn)

shales (2.77–2.83 a.f.u.).The calculated temperatures of the metasomatic shales are above those calculated for the rest of the rocks, having a mean of 419 ± 18 °C and a total range of 386–454 °C (Fig. 6b).

Carbonate minerals from the mafic volcanic rocks (M3 sample) consist of Fe-bearing dolomite or Fe–Mg calcite (Table 2). Data from EMPA is projected in the triangular diagram Fe–Ca–Mg where the fields of solid solutions and carbonate phases are shown for $T \approx 250–400$ °C (Rosenberg 1967; Anovitz and Essene 1987) (Fig. 6c). The analyzed carbonates project in the two-phase field of coexistence between calcite (Cc) or Mg-calcite solid solution phase (Mg-Cc_{ss}) and

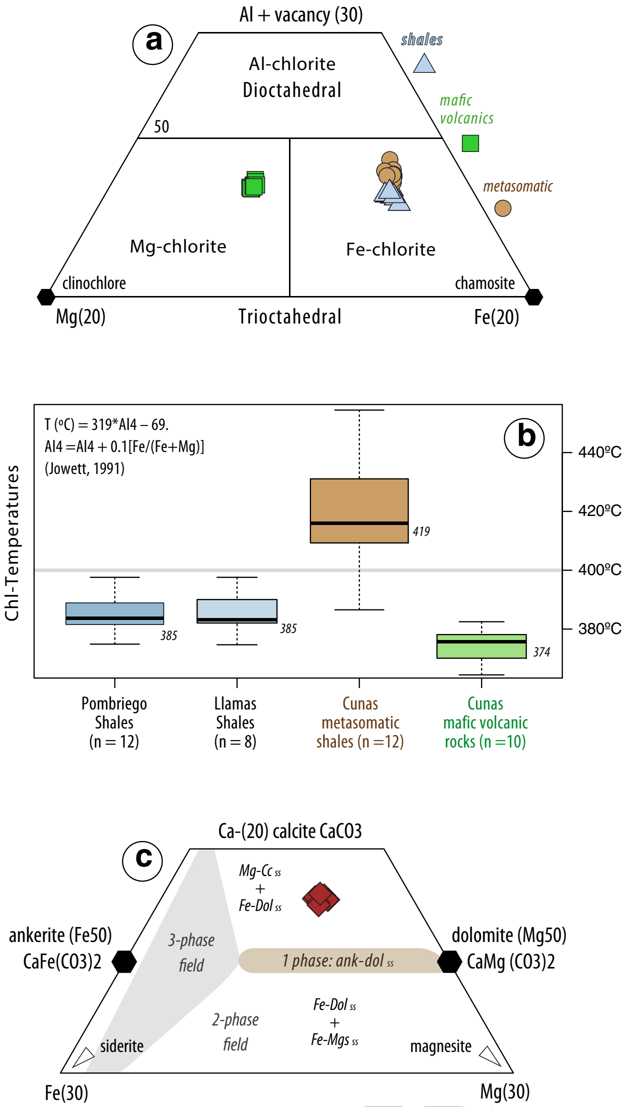

Fig. 6 Chlorite and carbonate mineral chemistry. **a** Chlorite classification by Zane and Weiss (1998). **b** Chlorite temperature calculations by the method of Jowett (1991). Chlorite data from the host shales, sampled in other localities, was projected for comparison (unpublished data from Gómez-Fernández. See Table 1 for average values). **c** Ca–Fe–Mg diagram with the projection of the studied carbonates

Fe-dolomite solid solution phase (Fe-Dol$_{ss}$). The analyzed carbonates would not represent therefore a single phase but a mixture of these two phases.

7 Geochemistry

The studied samples consist of volcanic-volcanoclastic and metasomatic shales (Table 3). The volcanic and volcanoclastic rocks show SiO_2 contents of 39.43–44.89 wt.% (average: 42.75 wt%) and $Na_2O + K_2O$ of 3.7–5.5 wt%. Their MgO (6.76–9.14 wt %), FeOt (10.45–11.40 wt%) and CaO (2.07–7.30 wt%) range from moderate to elevated values. Their TiO_2 contents are also high (1.84–2.48wt.%). These features allow classifying these rocks as basalts, trachybasalts and basanites. Two of them have slightly anomalous A/CNK values (C-2 = 1.06, IGS-40 = 1.17), probably due to alteration and partial Ca loss. Regarding trace elements, these rocks have elevated Ti/Y (500–100), Nb/Y (1.5–2.5), Th/Yb (1.5–2.5) and Nb/La (1–1.5) ratios, indicative of their alkaline affinity. They plot in the field of within-plate basalts (Fig. 7a) suggesting absence of subduction/crustal contamination.

Within this volcanic-volcanoclastic group, sample C-7 makes a difference due to its felsic nature: $SiO_2 = 74.50$ w.%, $Na_2O + K_2O = 2.94$ wt%, very low CaO content (0.10 wt%), moderate to high MgO (0.82 wt%) and very high peraluminosity (A/CNK = 3.81). This rock can be classified as a rhyolite with a greywacke volcanoclastic composition, following the criteria of Herron (1988) (Fig. 7b).

The metasomatic shales have a wide SiO_2 range of 33.90–58.10 wt%, with the lowest SiO_2 values within the sheared samples (Table 3). The most striking attribute of this group of rocks is the high FeOt content (20.40–32.70 wt%; average: 24.48 wt%). The Al_2O_3 concentration is heterogeneous but relatively high in some cases (11.75–23.80 wt%, average: 17.34%). Due to the very low CaO, Na_2O and K_2O abundances (< 1wt%), the A/CNK values of these rocks are quite variable and very high (5.52–36.52), being extremely peraluminous. Positive correlations exist between FeOt and TiO_2, Nb, Sc and HREE. Due to its very high FeOt/K_2O (log values: 0.91–2.67) and low SiO_2/Al_2O_3 ratios (log values: 0.20–0.66), these rocks could be classified as Fe-Shales (Fig. 7b) if a sedimentary origin is assumed.

The Luarca Formation, composed of shales-slates, host the volcanic rocks and the metasomatic shales (Ward and Gómez-Fernández 2003).These shales-slates have relatively low contents of SiO_2 (49.55–55.27 wt%) and CaO (0.18–0.72 wt%), and high Al_2O_3 (23.17–26.08 wt%) and FeOt (8.28–10.59 wt%) compared to standard shales (Fig. 7b). Their A/CNK is high (3.14–3.97), thus being very peraluminous rocks. The SiO_2/Al_2O_3 ratio is low (log values: 0.27–0.45) while the FeOt/K_2O is slightly high (log values: 0.30–0.52) (Fig. 7b). These geochemical features allow us to classify these rocks as shales plotted close to the limit with Fe-Shales and being more Fe-rich compared to standards such as NASC (North American Shale Composite, Gromet et al. 1984) and PAAS (Post Archean Australian Shale, Taylor and McLennan 1985).

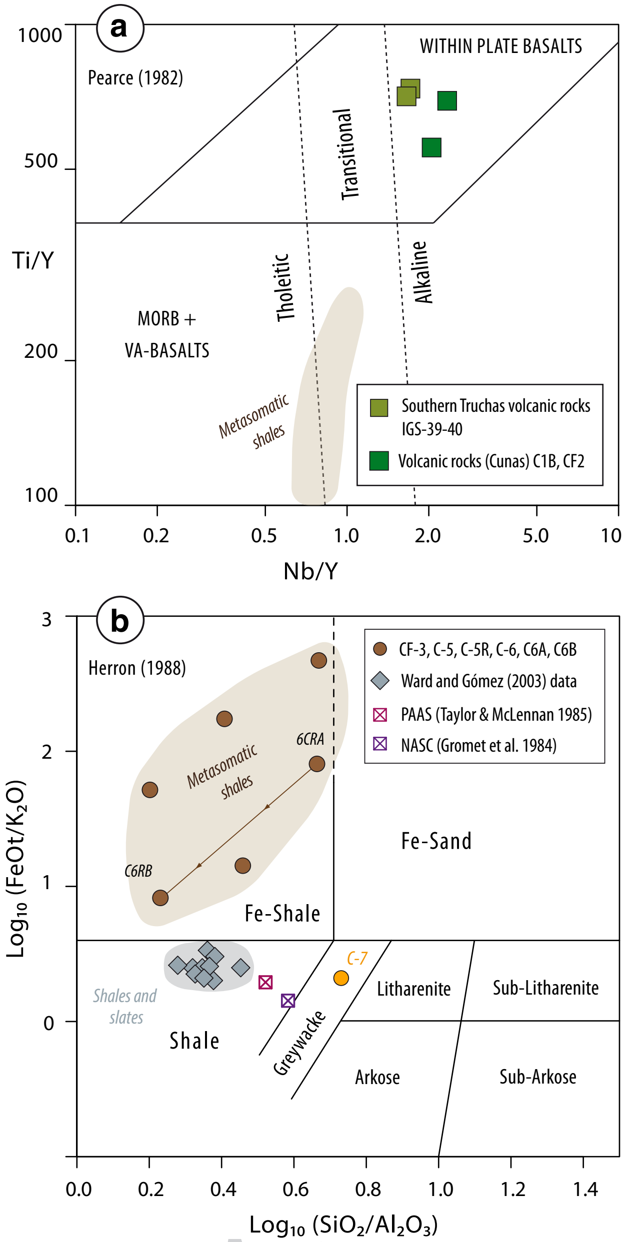

Fig. 7 Classification diagrams used for the volcanic and metasomatic shales. **a** Tectonic setting diagrams based on the Ti/Y and Nb/Y ratios (Pearce 1982). **b** Classification diagram for sedimentary rocks (Herron 1988)

7.1 Rare earth elements

The contents and patterns of measured rare earth elements (REE) show significant differences between the different rocks studied (Fig. 8). The mafic volcanic rocks show a fractionated pattern with La/Yb normalized values of 10.35 on average and very low to absent Eu negative anomalies ($Eu^* = [Eu_n/(Sm_n{*}Gd_n)^{\wedge 0.5}] = 0.97$ on average). These data

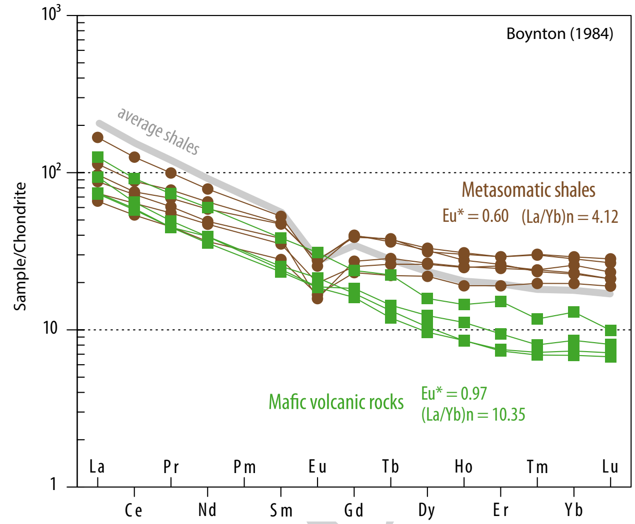

Fig. 8 Rare earth element normalized to chondrites (Boynton 1984) for the studied volcanic and metasomatic shales and average host shales (unpublished data from Gómez-Fernández–average in Table 3)

together with the heavy rare earths (HREE), below 10× chondrite values, are typical features of alkaline basalts.

The REE patterns of the metasomatic shales are similar to those displayed by the shales, with light rare earths (LREE) fractionation and a flat HREE outline. The Eu anomaly of these rocks is moderate ($Eu^* = 0.60$) and very similar to that shown by the host shales (Eu*Luarca Shales = 0.63). On the contrary, the average fractionation of the REE is low ($La_n/Yb_n = 4.12$) and somewhat different to that of shales (La_n/Yb_n Luarca Shales = 11.56).

7.2 Comparison to bulk continental crust composition

Spider plots normalized to the bulk continental crust of Taylor and McLennan (1985) are presented in Fig. 9. These show the differences and similarities of the trace element contents between the volcanic, metasomatic and shale rocks. The volcanic rocks show typical depletions in large ion lithophile (LIL) elements such as Rb, K, Ba and Cs, whereas Th and U are similar to the bulk crust. High field strength (HFS) elements (Nb, Ta, Sr, Zr, Hf, Ti) and LREE show values above the bulk crust. On the other hand, the HREE are below typical crustal values. The LIL elements of the metasomatic shales display a pattern intermediate between volcanic and shale compositions, with very variable K depletions and the same Th and U values as the shales. Regarding the HFS elements, the metasomatic shales have similar Nb–Ta relations to the volcanic rocks and closely similar Zr-Hf pattern as the shales. Negative Ti anomalies and a strong Sr depletion are common features with the shales. The REE pattern is more

Journal : Large 41513	Article No : 147	Pages : 23	MS Code : 147	Dispatch : 9-11-2020

Fig. 9 Spider diagrams normalized to the bulk continental crust ▶ (Taylor and McLennan (1985). Shales data from Gómez-Fernández (unpublished average in Table 3) are compared to the studied metasomatic shales and volcanic rocks. Grey field is the total range of the data

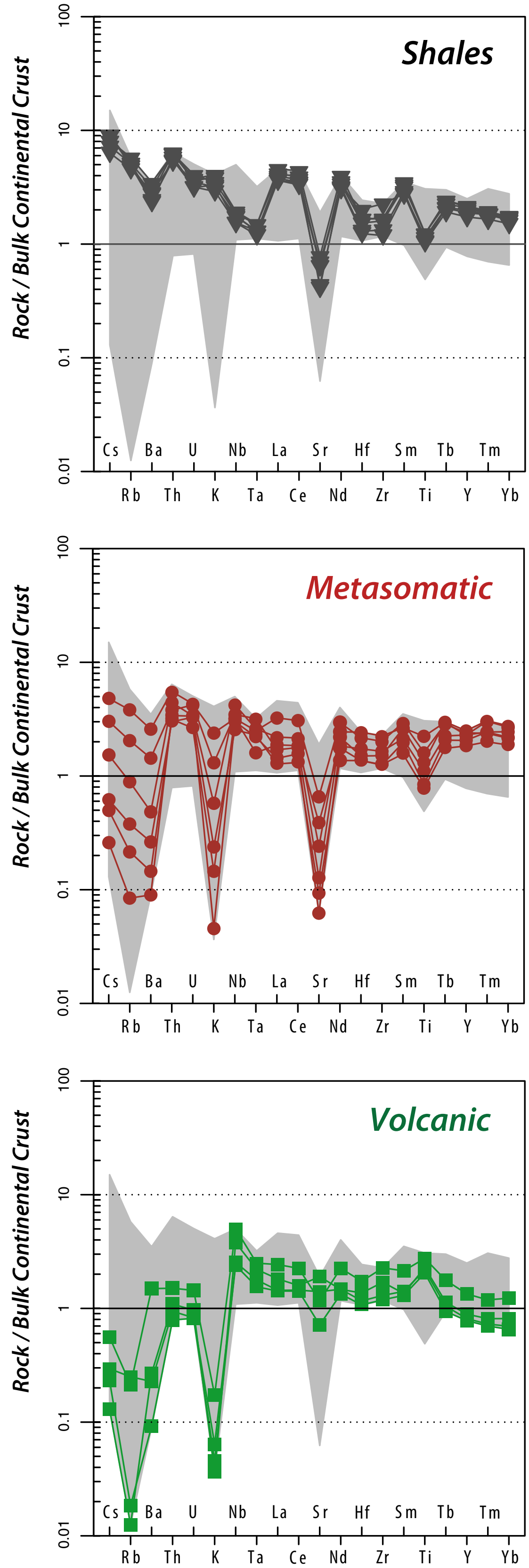

similar to that of the shales but with slightly lower and variable LREE and higher HREE values.

8 Discussion

8.1 Nature of the mantle source and geodynamic context

The studied Ordovician volcanic rocks from the Truchas Syncline have a geochemistry similar to OIB and within-plate basalts (Figs. 7a and 10). The main difference with OIB composition is the LILE depletion: Rb, K and variably Ba negative anomalies. No features of subduction or important crustal contaminations (Nb–Ta–Ti negative anomalies) are observed, except for some slight positive Pb anomalies (Fig. 10). Other Ordovician basalts and basalts of supposed post-Variscan age (Valverde-Vaquero et al. 2016; González Menéndez and Suárez, 2004) show a similar OIB-type pattern but with substantial differences in LILE compared to the studied Truchas basalts. The whole set of these basalts, even with their age differences, could have had a similar initial geochemistry affected by different processes: (i) More or less LILE enriched basalts whose content was later increased by hydrothermal fluids (González Menéndez and Suárez 2004) and (ii) subsurface/seafloor alteration and LILE leaching in the Truchas volcanic rocks. Other Iberian post-Variscan mafic dikes (Permian to upper Cretaceous) have a similar geochemistry except for the LILE depletions of the Truchas volcanic rocks (Gallastegui and Cuesta 2005; Orejana et al. 2008). The source of the studied Truchas basalts was probably a relatively enriched mantle unaffected by previous subduction processes. This protolith experienced low melting degrees. This is in agreement with the observed HFSE and REE fractionations and supports a tectonic regime of incipient rifting and lithosphere thinning.

8.2 Carbonate phases in the volcanic rocks: seafloor alteration vs. hydrothermalism—metamorphism

Carbonates in some of these volcanic rocks are of interest because their origin could be related to H_2O–CO_2 late-stage metamorphic fluids and these could act as transport agents of dissolved Au (Phillips and Evans 2004). Nevertheless, different hypotheses need to be considered in the first place.

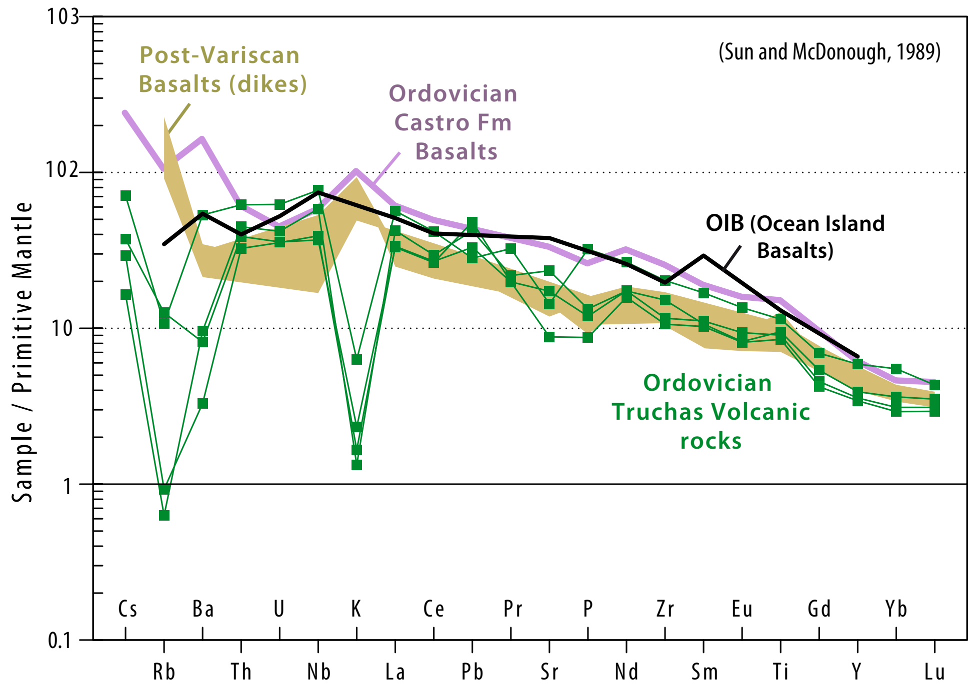

Fig. 10 Primitive mantle normalised trace element composition of the Truchas Syncline basalts. The shaded field corresponds to north Spain´s post-Variscan basaltic dikes (González Menéndez and Suárez 2004). Ordovician Castro Fm. basalts are from Valverde-Vaquero et al. (2016). OIB average values are from Rollingson (1993) and references therein. Normalising values of primitive mantle are from Sun and McDonough (1989)

(i) The composition of the studied volcanic rocks is mainly mafic (basaltic) and their correspondent magmas could have considerable CO_2 contents due to the high solubility of this phase in mafic magmas (King and White 2003). Nevertheless, volcanic rocks degas relatively fast, during and after emplacement, because of its low viscosity (Sparks 2003) implying that CO_2 deriving from the volcanic rocks is an unlikely source of CO_2 in carbonates.

(ii) The studied volcanic rocks were emplaced into a shallow marine sedimentary basin, where Ordovician shales were being deposited. In this paleo-environment, carbonates could have formed by chemical precipitation from seawater and by alteration of Ca-bearing phases within the volcanic rock. Seafloor alteration/precipitation should have produced calcite as the main carbonate (± chlorite ± albite) and this typically occurs on previous Ca-bearing minerals, fracture fillings and rock-vesicles (Groves et al. 1988). Furthermore, if this hypothesis is correct, most these volcanic samples should have carbonate phases because they have a fairly homogeneous basaltic composition and were expelled in the same marine environment and were exposed to the same seafloor alteration conditions. Of the different studied samples, three have carbonate phases replacing primary plagioclase (Fig. 5).

(iii) Crustal fluids, produced by metamorphic dehydration in deeper crustal locations, are composed of $H_2O + CO_2$ (± other minor salt components). These fluids usually traverse upper crust formations where they cool and crystallize as quartz veins. Interaction with rocks that have Ca–Mg–Fe can lead to precipitation of different carbonates phases. The presence of Fe-dolomite, Mg–Fe calcite, ankerite and/or magnesite-siderite, besides calcite, should be indicative of metamorphic/hydrothermal processes (Groves et al. 1988).

The petrography study shows that undeformed carbonates substitute chlorite and also appear in veins crosscutting the chlorite matrix (Fig. 5b–d). The observed carbonate compositions of Fe-bearing dolomite/Mg calcite favors a metamorphic origin for the fluids (Groves et al. 1988). These data thus support an origin of these carbonates as precipitates from crustal fluids generated after the chlorite ($\approx 374 \pm 6$ °C) metamorphic growth. These fluids can flow through the crust in a pervasive way, or, more commonly, in more discrete zones where the fluids are collected. This could explain why some mafic volcanic rocks developed carbonate phases while others did not. Another possible explanation is that minor heterogeneities in the studied basalt compositions could have limited/augmented the availability of reactants and thus conditioned the development of carbonate phases.

8.3 T-X(CO_2) modelling in the volcanic rocks

Phase diagram (pseudosection) modelling in the system NCaKFMASHC was done to investigate the formation of

Journal : **Large 41513**	Article No : **147**	Pages : **23**	MS Code : **147**	Dispatch : **9-11-2020**

carbonate phases by crustal fluid ($H_2O + CO_2$)—rock interaction. The thermodynamic data base ds.55 of Holland and Powell (1998) was used together with the following A–x solution models: muscovite (Coggon and Holland 2002), biotite (White et al. 2007), chlorite (Holland et al. 1998), amphibole (Diener et al. 2007) and feldspar (Holland and Powell, 2003). Carbonate phases calcite-dolomite-magnesite (CcDo) were treated as a solid solution phase with the model of Holland and Powell (2003). Ankerite and siderite were considered as pure end members. The Pitzer and Sterner (1994) equation of state was considered for modelling the $H_2O–CO_2$ (site mixing) behaviour.

Theriak-Domino software (De Capitani and Petrakakis 2010), a Gibbs free energy (G) minimization code, was used for calculations and diagrams. The input bulk rock-composition is the sample CF2, representative of the volcanic rocks with basaltic composition from the studied area (Table 3).

The results are presented in a T-XCO_2 equilibrium phase diagram or pseudosection where temperature (T) is compared to $XCO_2 = nCO_2/nH_2O + nCO_2$. The model was generated with a fixed pressure of 1 kbar to model near surface conditions (Fig. 11). Stable phase assemblages with the lowest G values for the specific P–T–X conditions are shown. High contents of $H_2O–CO_2$ were considered in order to have fluid in excess. At the T range studied (300–400 °C) the observed assemblage of albitic Pl + Chl + Fe-dolomite/Mg-calcite ± sericite ± Qtz ± K-feldspar is best matched by the calculated assemblage of Pl(Ab) + Chl + CcDo + Ms-Pg ± Qtz shown in the colored field of Fig. 11. The T-XCO_2 conditions for this field are varied because it has a positive slope and therefore spans a considerable range of T (≈ 200–360 °C) and XCO_2 (0.05–0.47). Higher T values or lower XCO_2 fluid composition will generate biotite as a stable phase in the assemblage. Higher XCO_2 contents will lead to the increase of ankerite ± siderite as the main carbonate phases. The calculated modal amounts of the mineral assemblage are close to those observed where Pl(Ab) + Chl dominate (calculated Pl ≈ 42%, Chl ≈ 35%) followed by the carbonates (calculated CcDo + Ank ≈ 11%) and sericite phases (Ms + Pg ≈ 10%). Carbonates are slightly underestimated while sericite phases are overestimated compared to the observed modal amounts.

With this model we can only establish a maximum T (≈ 350–360 °C) below which the observed mineral assemblage was developed in a range of possible fluid XCO_2 values. This temperature is slightly lower than the one recorded

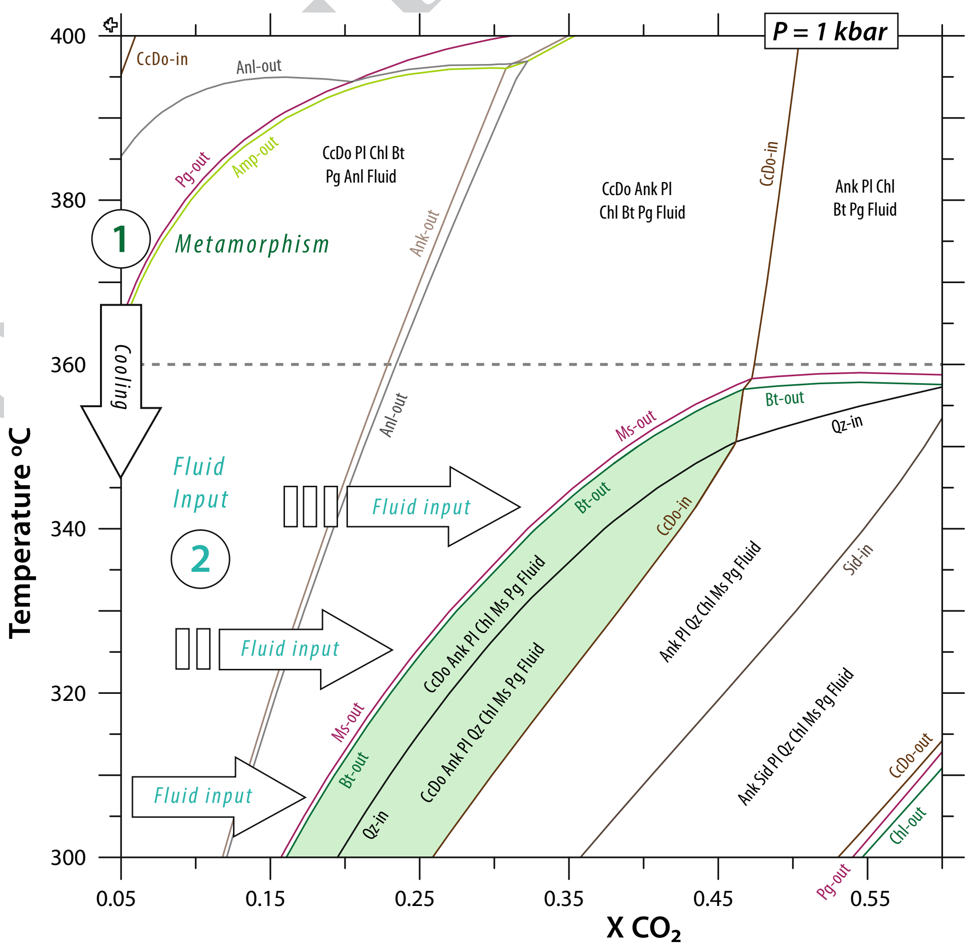

Fig. 11 T-XCO_2 Pseudosection at P = 1 kbar. Mineral abbreviations—*Pl* plagioclase, *Chl* chlorite, *CcD* calcite-dolomite, *Ank* ankerite, *Sid* siderite, *Ms* muscovite, *Pg* paragonite, *Anl* analcime, *Qz* quartz, *Amp* amphibole. Bulk rock in cation mol proportions is Si(71.39), Al(35.68), Mg(16.77), Fe(15.87), Ca(7.98), Na(17.19), K(0.40), C(1000-0), H_2O(0-1000). Stage 1 refers to the temperature estimated (Chl composition) for the low-grade metamorphic event. Stage 2 refers to the possible input of fluid $H_2O–CO_2$ input into the rock. See main text for further explanations

Journal : Large 41513	Article No : 147	Pages : 23	MS Code : 147	Dispatch : 9-11-2020

in the chlorite compositions (≈ 374 °C) related to low-grade metamorphism (low greenschist facies). This, and the textural relations of carbonates, overprinting or cutting across the chlorite crystals, indicates that the growth of the carbonates took place at relatively lower temperatures and was an event of fluid (H_2O–CO_2) infiltration that occurred after or during the waning stages of the low grade regional metamorphism.

Therefore, we propose a regional metamorphic event at stage 1 at T ≈ 374 ± 6 °C (Fig. 11). The XCO_2 fluid values were low ($XCO_2 \leq 0.025$) and carbonate phases were either not stable or had very low modal abundances. This is supported by the fact that no chlorite-carbonate intergrowths or simultaneous chlorite-carbonate growths were observed in the samples. After this event and during cooling below ≈ 350–360 °C, an H_2O–CO_2 fluid input occurred at stage 2 (Fig. 11). This caused the development of carbonates as crystals and veins cutting across the rest of the phases. The fluid composition could have been buffered by the breakdown of biotite to form muscovite/sericite. Although there are no records of this reaction in the rocks, if it had occurred, fluid chemistry would have changed upon cooling and exhumation of the rock and would have been buffered along the Bt-out reaction line in Fig. 11. Such behavior of changing fluid composition upon pervasive fluid infiltration is not uncommon in metamorphic rocks (Kleine et al. 2014).

Other scenarios where infiltration of H_2O–CO_2 crustal fluids interacted with mafic rocks to produce carbonation and, in some cases, Au mineralization, have similarities and differences with the model here described.

A similar evolution was proposed by Kleine et al. (2015) and Kleine et al. (2016) in metabasaltic sills from Islay (Scotland) with H_2O–CO_2 infiltration fluids being synmetamorphic (but post peak) and carbonation only affecting the sill margins. On the other hand, a different sequence of events is proposed in the model of Elmer et al. (2007) where an Au-hydrothermal event and H_2O–CO_2 fluid infiltration took place before the metamorphic peak conditions (440 °C).

In our study case it seems that the infiltration of H_2O–CO_2 fluids and carbonation of the mafic rocks happened after the metamorphic peak (chlorite average temperature ≈ 374 ± 6 °C) or during the waning stages of metamorphism. This is mainly based on the observation of carbonates minerals and quartz-carbonate veins cut across chlorite minerals (Fig. 5b–d).

H_2O–CO_2 fluids, with the suitable ligands (HS, Cl^-), are known to be carriers of dissolved gold as bisulphide $(Au(HS)^-{}_2)$ of chloride complexes $(AuCl^-{}_2)$. The observed Au mineralization in this region (Truchas Syncline) could be related to this H_2O–CO_2 input. The relatively moderate temperatures estimated for this fluid (< 350–360 °C) are similar to those described in Au mineralization fluids from other regions (≥ 200–300 °C; Phillips and Evans 2004; Phillips and Powell 2010).

8.4 Origin of the metasomatic shales

Previously, the lithological layers that we classified as metasomatic shales in this study were reported to be of volcanic origin (Suárez et al. 1994). However, here we show evidence that these rocks lack chilled margins, scoriaceous upper layers or observable igneous textures such as phenocrystals (Fig. 4). In thin section, the mineral assemblage observed is chlorite + quartz ± rock fragments and accessory zircon (Fig. 5e,f) which casts doubts about a sole volcanic origin. The chlorite chemistry (Fig. 6) and whole rock geochemical data indicate an origin closer to a shale ± sandstone composition with a minor volcanic component (Fig. 9).The rare composition of these rocks indicates that they are neither volcanic (igneous) nor completely sedimentary and instead, should be considered as metasomatic. The more deformed samples have low $FeOt/K_2O$ and SiO_2/Al_2O_3 ratios and the deformation effect on the geochemistry is shown in Fig. 7b (deformation trend).

To further explore its geochemistry, we performed principal component analysis (PCA) including the whole set of studied rocks: metasomatic, volcanic and shale compositions (shales from Ward and Gómez-Fernández 2003 and unpublished data from Gómez-Fernández). PCA shows the geochemical variance grouped in a small set of components. The first two components account for 75% of the variance (Fig. 12a). The first one is dominated by the variables that separate the geochemistry of volcanic rocks from that of the shales: SiO_2, Al_2O_3, and K_2O typical of the shale compositions and CaO, MgO, TiO_2 and Na_2O that correspond to the mafic rocks. Metasomatic shales are closer in this 8-dimensional space to the shales. The second component is dominated by Fe_2O_3t negative loading with minor contributions of K_2O, $Na_2O \pm SiO_2 \pm Al_2O_3$. This shows the importance of the iron enrichment in these rocks accompanied with a decrease in alkalis (Na_2O, K_2O). This alkalis decrease, without an accompanying Al_2O_3 increase, is responsible for the extreme peraluminosity of these rocks. Within the metasomatic shales, there is also a high SiO_2 variability (Fig. 12b).

A high affinity of the metasomatic shales and shale compositions can also be seem with the Th and La diagram (Fig. 13). The Th/La ratios of these rocks are closer to those of zircon (0.35) and monazite (0.32) and different from those defined by the volcanic whole-rock data. We have also performed isocon analysis (Grant 1986; 2005) considering both a shale source (average composition in Table 3) and a volcanic protolith (CF-2) to generate an altered metasomatic rock (CF-3). The 1:1 isocon black line and the isocon dashed lines obtained considering TiO_2, Zr and MnO as immobile elements were used to define the region of

Journal : Large 41513	Article No : 147	Pages : 23	MS Code : 147	Dispatch : 9-11-2020

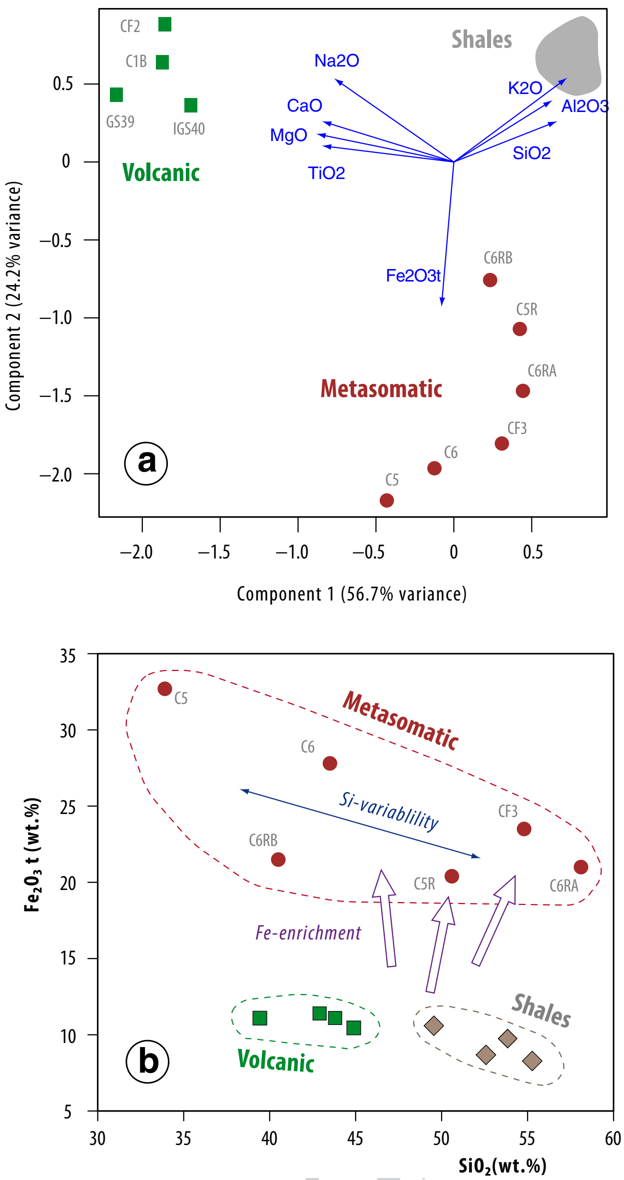

Fig. 12 **a** Results of Principal Component Analysis (PCA) of the whole data set (variables: major elements). In the bi plot, vectors express the correlations of the variables to the principal components: variables that are close to the center of the plot are less important (lower loading) for the first components. The Individual samples contribution to variance is projected as well. A sample that is on the same side of a given variable (vector) has a high value for this variable. **b** SiO_2 vs. Fe_2O_3t showing both the Fe- enrichment and Si variability of the metasomatic rocks compared to both the shales and volcanic rocks

least element mobility (Fig. 14).The results show that in all cases the metasomatic rocks gained $Fe_2O_3t \pm Nb$ (shale precursor) or $Fe_2O_3t + Pb \pm SiO_2$ (volcanic precursor). On the other hand, there are net losses in: K_2O, Na_2O, CaO, Rb, Sr, Ba, and LREE (shale precursor, Figs. 14a, b) or CaO, Na_2O, MgO, Sr, Ba, V (volcanic precursor, Fig. 14c, d).

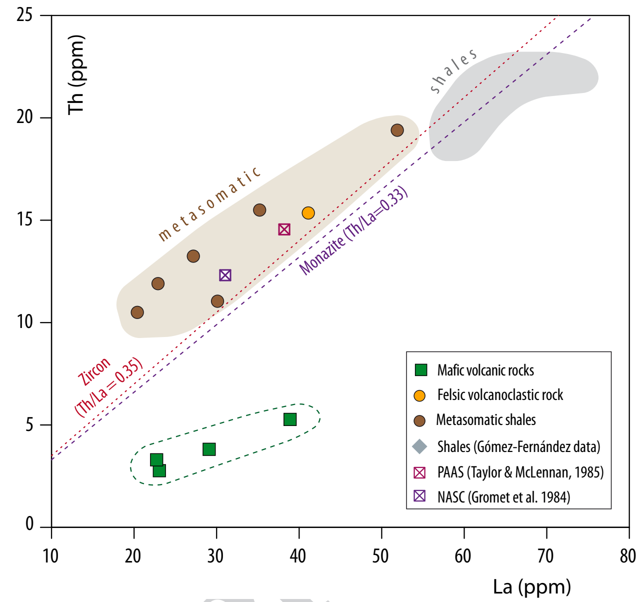

Fig. 13 Th vs. La diagram showing the whole rock variability of volcanic, metasomatic, host shales and standard shales. Zircon and monazite Th/La ratios are projected as dashed lines for comparison

The common ground is the marked Fe enrichment and the $Na_2O + CaO + Sr + Ba$ depletions.

Some of the borders of the metasomatic shales appear strongly foliated in comparison with its interior. We sampled both parts to investigate if there was any geochemical difference (from the border to the interior: C-6RB, C-6, C-6RA; Fig. 15). Since these rocks have a volcanic component, primary mineral-geochemical relations need to be considered. Mineral redistribution during a volcanoclastic emplacement could involve enrichments in Al, Si, Na, Ba, Rb and Sr in the body interior and higher concentrations of Ti, Fe, Mg, Mn, HFS elements and REE towards the margins (Kleine et al. 2016). In the study profile we have normalized the margin rocks (foliated) to the interior sample (Fig. 15). The most marginal and foliated sample (C-6RB) shows depletions in $SiO_2 \pm MnO$ and enrichments in most of other elements, especially in TiO_2, Al_2O_3, CaO, Na_2O, K_2O, Rb, Sr, Ba and LREE. Overall, this pattern is not consistent with a magmatic mineral-element redistribution. The geochemistry variation from the rock core towards the edges does not have a specific trend because the intermediate sample (C-6) does not have an intermediate geochemistry. The strong foliation observed suggests that the shearing associated with Variscan tectonics might have modified the chemistry of the rock margins by dissolving SiO_2 rich minerals (mainly quartz ± feldspars) with pressure solution and leached SiO_2 locally from the most deformed rocks. The rest of the elements would have had less mobility in these conditions and therefore increased its concentration by a corresponding residual enrichment.

Journal : Large 41513	Article No : 147	Pages : 23	MS Code : 147	Dispatch : 9-11-2020

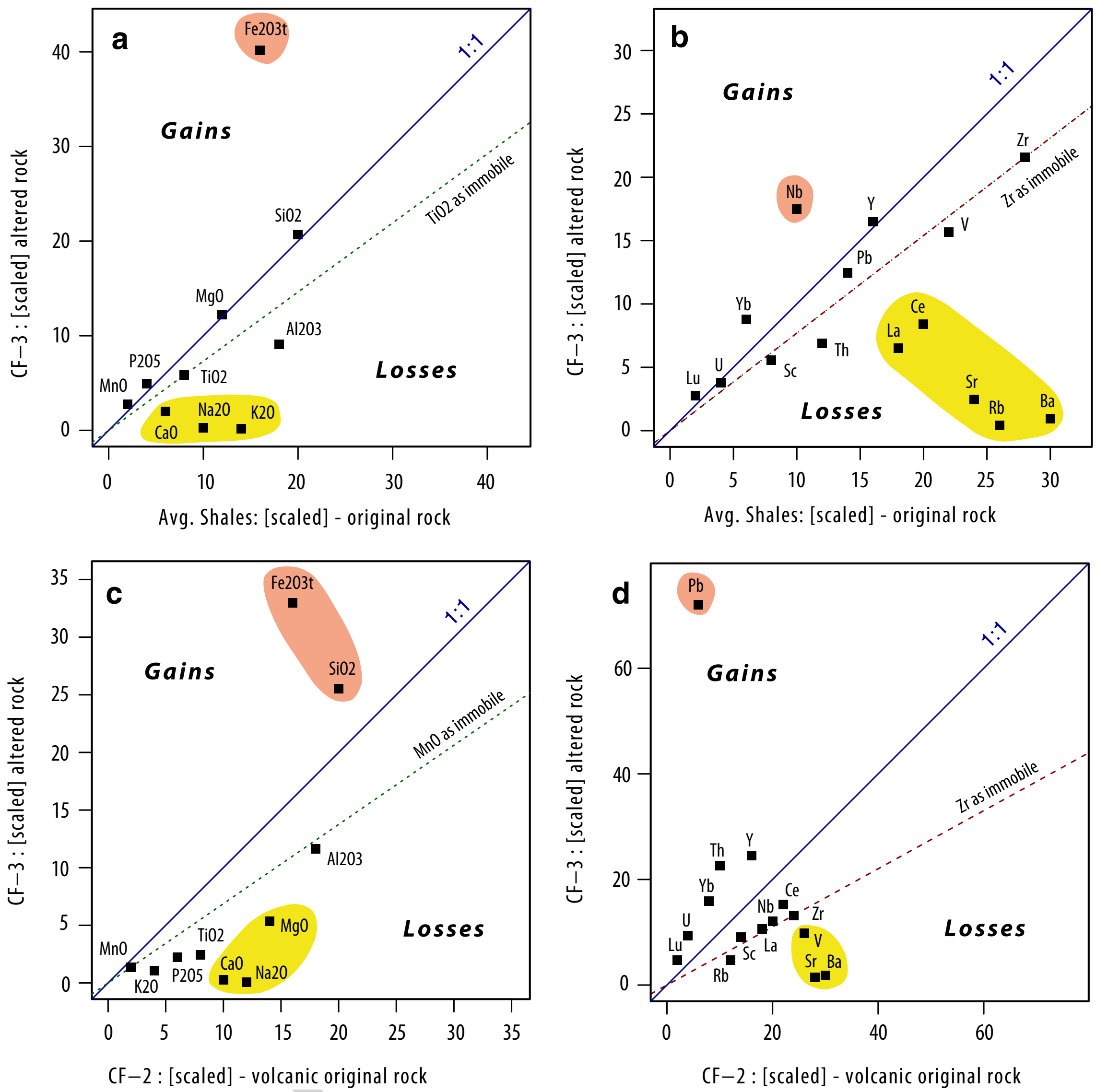

Fig. 14 Isocon diagrams (Grant 1986; 2005) of the average shales (**a**, **b**) and volcanic rock CF-2 (**c**, **d**) as possible protoliths (original rocks) for the metasomatic shales (CF-3 altered rock). The solid line is the 1:1 reference line. Dashed lines are the slopes based on possible immobile elements (Ti, Zr, MnO)

8.5 Sequence of geological processes

The data here presented, from field observations, petrography, geochemistry and T-XCO_2 modelling, suggest that these Ordovician volcanic rocks were emplaced in a relatively shallow marine basin as lavas and volcanoclastic deposits. Very rapid cooling generated the scoriaceous layers characteristic of some of these rocks. The magma composition could have been mafic with minor dacitic-rhyolitic pulses. The rapid cooling of these bodies, due to their relatively small thickness, precluded a metamorphic aureole development in the country rock shales. Preservation of orthid brachiopods in some volcanoclastic layer reinforces a Middle Ordovician age and a shallow marine setting for the volcanic deposits.

Possible seafloor alteration is mostly obliterated by the later Variscan metamorphism. It probably consisted in some chlorite ± albite development. This process could have affected all these volcanic rocks in a similar way and with similar intensity.

The metasomatic shales, previously mapped as volcanic layers, probably represent a mixture of shales ± sandstones and minor volcanic components. The significant SiO_2 depletion in the foliated rock margins could have happened by mineral dissolution (quartz ± feldspars) produced by the later Variscan deformation (shearing).

Journal : Large 41513	Article No : 147	Pages : 23	MS Code : 147	Dispatch : 9-11-2020

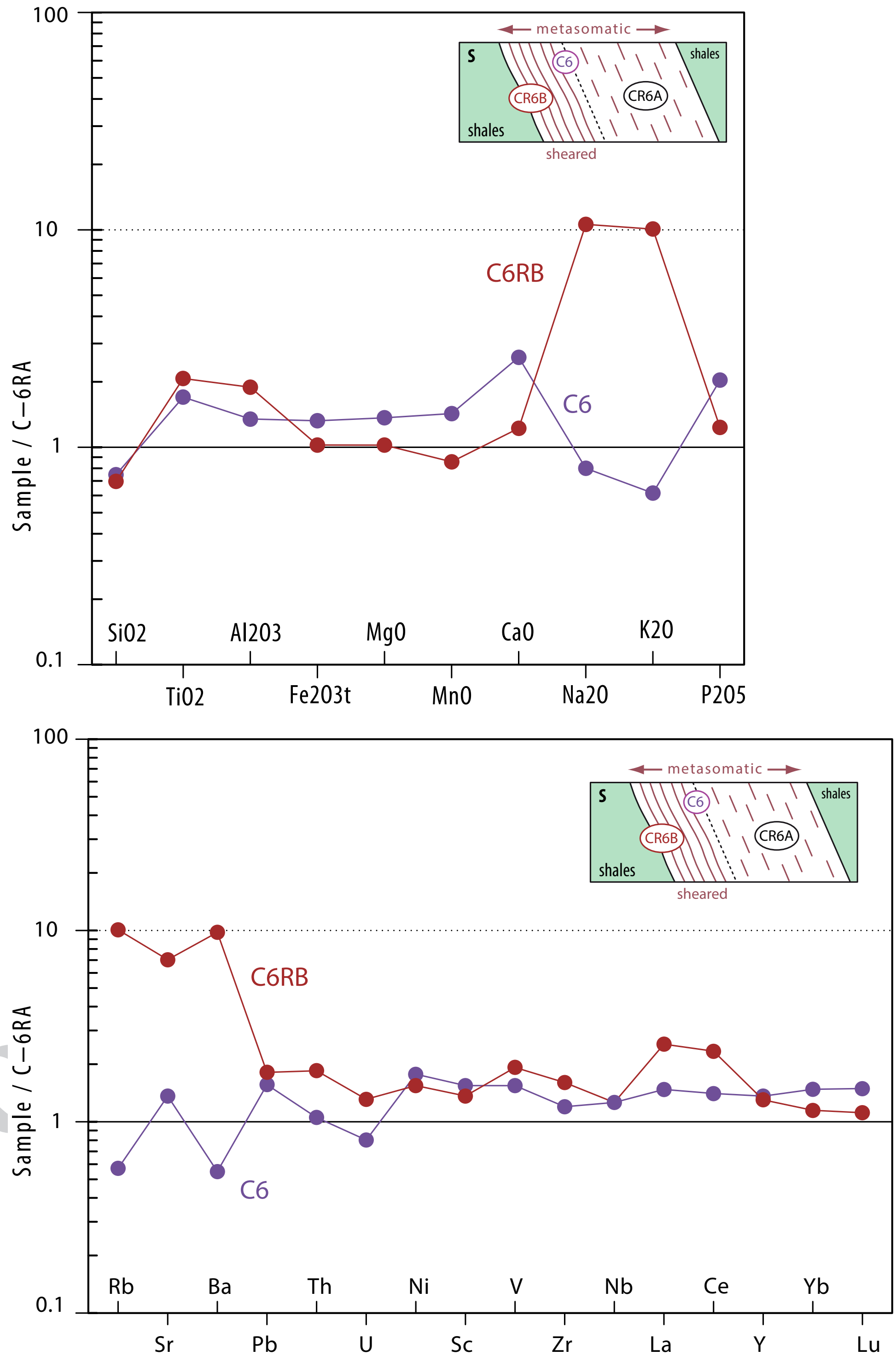

Fig. 15 Major and selected trace elements composition of the foliated metasomatic shales (C-6, C-6RB) normalized to the less deformed, non-foliated sample (C-6RA). Insets show the relative position of the samples in the outcrop

The Variscan Orogeny folded and metamorphosed these rocks up to greenschist grade as recorded in the Chl temperature estimations (≈ 374 ± 6 °C). We propose that, during this orogenic event, after the metamorphic peak, crustal H_2O–CO_2 fluids flowed through some of these volcanic rocks and produced fluid-rock interactions with Ca–Fe–Mg minerals at hydrothermal temperatures (< 350–360 °C). Depending on the XCO_2 of the fluid, different carbonate phases could have been produced (as shown in the modelling of Fig. 11). Gold could have been leached and transported by some of these fluids, giving rise to economic gold precipitation in some specific locations. The occurrence of carbonate phases in some of the country rocks (sedimentary/volcanic; Gómez-Fernández et al. 2009) could indicate the passage of

Journal : Large 41513	Article No : 147	Pages : 23	MS Code : 147	Dispatch : 9-11-2020

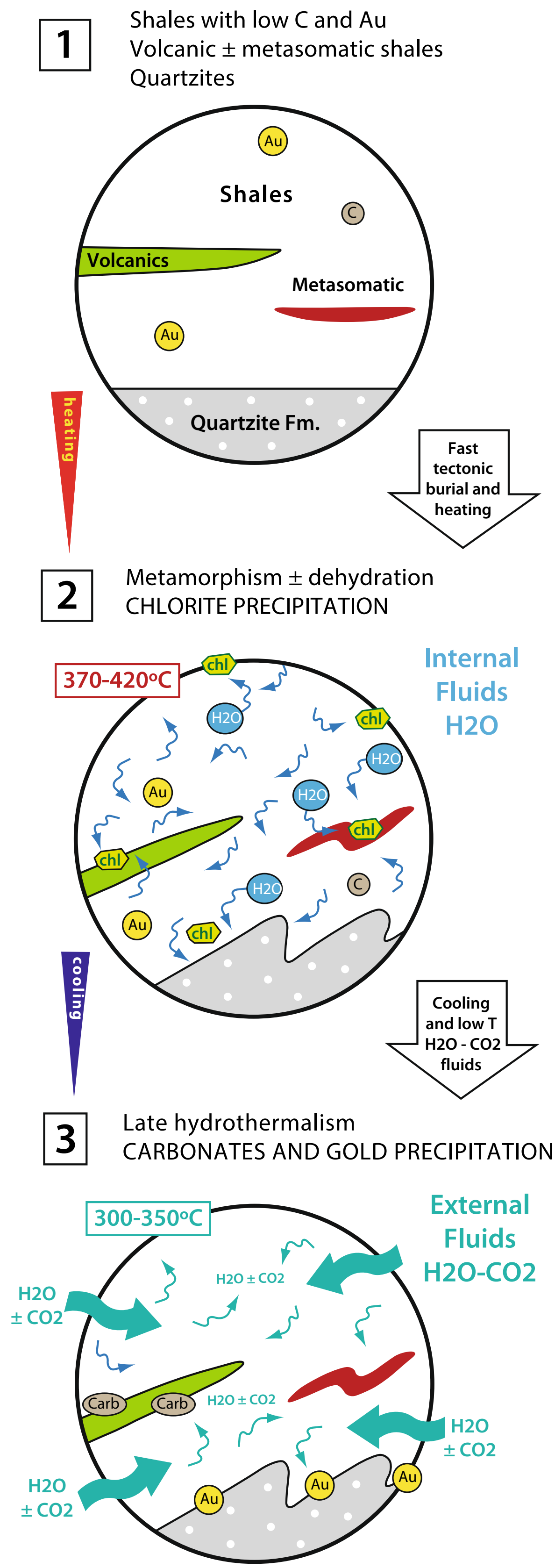

Fig. 16 Conceptual model in three stages for the Variscan metamorphism and late hydrothermalism that led to the carbonate precipitation and possible gold mineralization in the studied zone. See the main text for explanations

crustal fluid with mixtures of H_2O–CO_2 that can also carry dissolved Au to produce mineralization.

Based on the data presented, a conceptual model has been described showing the possible evolution of these rocks in relation to the Variscan metamorphism, carbonate precipitation and gold mineralization (Fig. 16). In a first stage, the original upper crustal rocks of this zone were composed of volcanic + volcanoclastic layers ± metasomatic layers and surrounding shales (Fig. 16). The shales have low initial amounts of organic C and dispersed low amounts of Au among diagenetic pyrite (Gómez-Fernández et al. 2019; Cunningham et al. in prep). The Variscan orogeny produced heat leading to T increases up to ≈ 374–420 °C. This caused a widespread chlorite precipitation from dehydration reactions of previous phyllosilicate minerals within the shales and metasomatic rocks. Interactions of these H_2O-rich fluids with the volcanic and metasomatic rocks produced a retrograde metamorphism of mafic minerals of the volcanic rocks and in the volcanic components of the metasomatic rocks (Fig. 16, stage 2). The low C content of the shales probably precluded the generation of $H_2O + CO_2$ fluids at this stage, as indicated by the lack of carbonate phases growing simultaneously with chlorite. After the metamorphic peak, at the initial cooling stages (T ≤ 350–360 °C) infiltration of external and probably deeper $H_2O + CO_2$ fluids occurred. These fluids interacted with the different rock compositions (Fig. 16, stage 3). In the case of the volcanic rocks, having significant CaO contents (in plagioclase and mafic primary and secondary minerals), the reaction produced carbonate phases (Mg-calcite/Fe-Dolomite). The interaction of these fluids with the shales and metasomatic rocks did not cause carbonate precipitation because of the very low CaO contents of these rocks (0.08–0.36 wt%). For precipitation of pure Mg-Fe-carbonate phases (magnesite, siderite), higher XCO_2 (mole fractions) would be needed in the fluid. The gold mineralizations known around this area (Gómez-Fernández et al. 2012) could be related to these late $H_2O + CO_2$ fluids that transported dissolved Au (as bisulphide complexes $Au(OH)_2^-$). The ultimate origin of the gold is unknown, it could have been leached in part from the surrounding shales, and/or being leached from deeper geological settings where these late crustal fluids came from.

9 Conclusions

The Ordovician volcanic and volcanoclastic rocks of NW Spain are well represented in the Truchas Syncline and in the studied area of this work (SE Truchas Syncline, Cunas village). Here, these rocks are hosted and interbedded within Ordovician shales (Luarca shale Fm.) and mainly consist of within-plate alkaline basalts extruded in a marine passive margin. Such features are consistent with an extended passive continental margin linked to continental rifting processes.

Fossil occurrences (orthid brachiopods) within some of the volcanoclastic layers corroborate the Middle Ordovician age for these rocks and its shallow marine conditions of emplacement.

Metasomatic shales occur as distinctive layers within the shales succession. These chlorite + quartz rocks show important iron enrichments and extreme peraluminosity. Its protolith could be a shale ± sandstone with minor volcanic components.

Variscan greenschist metamorphism affected these rocks promoting the widespread chlorite growth at $T \approx 374 \pm 6$ °C, from primary mafic phases not currently preserved. Simultaneous deformation processes are observed in some cases where the chlorite has a slight preferred orientation.

Subsequent to this metamorphism and deformation, or in its waning stages, infiltration of H_2O–CO_2 fluids occurred through veins of variable scale and nature (Qz + Carbonate- and Carbonates-veins). These crustal fluids interacted with the volcanic rocks and particularly with its Ca–Fe–Mg phases, to produce carbonate minerals: Fe-bearing dolomite—Mg-bearing calcite at $T \leq 350$–360 °C. It is proposed that these H_2O–CO_2 fluids could have been responsible for the transportation and deposition of gold mineralizations located nearby.

Acknowledgements This project was partially funded by Project 0284_ESMIMET_3_E (INTERREG V-A Spain-Portugal Cooperation Programme, 2014–2020) and by Project LE167G18 (Junta de Castilla y León, Spain). We thank R. Arenas and P. Montero for editorial handling. We also thank B. Kleine and D. Orejana for their constructive comments and corrections that helped to improve the manuscript.

AQ2 **Funding** This project was partially funded by Project 0284_ESMIMET_3_E (INTERREG V-A Spain-Portugal Cooperation Programme, 2014–2020) and by Project LE167G18 (Junta de Castilla y León, Spain).

Compliance with ethical standards

Conflict of interest The authors declare that they have no conflict of interest.

References

Anovitz, L. M., & Essene, E. J. (1987). Phase equilibria in the system CaCO3-MgCO3-FeCO3. Journal of Petrology 2, 389–414.

Babin, C., & Gutiérrez-Marco, J. C. (1991). Middle Ordovician bivalves from Spain and their phyletic and palaeogeographic significance. *Palaeontology, 34,* 109–147.

Brendan Murphy, J., Gutiérrez-Alonso, G., Fernández-Suárez, J., & Braid, J. A. (2008). Probing crustal and mantle lithosphere origin through Ordovician volcanic rocks along the Iberian passive margin of Gondwana. *Tectonophysics, 461,* 166–180.

Boynton, W. V. (1984). Geochemistry of rare earth elements: meteorite studies. In P. Henderson (Ed.), *Rare earth element geochemistry* (pp. 63–114). New York: Elsevier.

Bucher, K., & Grapes, R. (2011). *Petrogenesis of metamorphic rocks*. New York: Springer.

Coggon, R., & Holland, T. J. B. (2002). Mixing properties of phengitic micas and revised garnet-phengite thermobarometers. *Journal of Metamorphic Geology, 20,* 683–696.

Diener, J. F. A., Powell, R., White, R. W., & Holland, T. J. B. (2007). A new thermodynamic model for clino- and orthoamphiboles in the system Na_2O–CaO–FeO–MgO–Al_2O_3–SiO_2–H_2O–O_2. *Journal of Metamorphic Geology, 25,* 631–656.

Díez Montes, A. (2007). *La geología del dominio "Ollo de Sapo" en las comarcas de Sanabria y Terra do Bolo*. Serie Nova Terra, nº34, 494 pp.

De Capitani, C., & Petrakakis, K. (2010). The computation of equilibrium assemblage diagrams with Theriak/Domino software. *American Mineralogist, 95,* 1006–1016.

Elmer, F. L., Powell, R., White, R. W., & Phillips, G. N. (2007). Timing of gold mineralization relative to the peak of metamorphism at Bronzewing, Western Australia. *Economic Geology, 102,* 379–392.

Emig, C. C., & Gutiérrez-Marco, J. C. (1997). Niveaux à lingulidés à la limite supérieure du Grès Armoricain (Ordovicien: Arenig) dans le SW de l'Europe: analyse des facteurs responsables et signification paléoécologique. *Geobios, 30,* 481–495.

Fernández-Lozano, J. (2012). Estudio geológico preliminar de un sector del cierre periclinal del Sinclinorio de Truchas (León): El anticlinal de Manzaneda. *Geogaceta, 52,* 17–20.

Gallastegui, G., Aramburu, C., Barba, P., Fernández, L.P. & Cuesta, A. (1992). El vulcanismo del Paleozoico Inferior de la Zona Cantábrica (NO de España). In: Rábano, J. C. Gutiérrez Marco, J. Saavedra (Eds.), *El Paleozoico Inferior de Ibero-América* (pp. 435–452). Gráficas Topacio, S.A., Madrid

Gallastegui, G., & Cuesta, A. (2005). Mineralogía y geoquímica de manifestaciones filonianas post-variscas en el NO de la Península Ibérica (Provincias de Lugo y León). *Macla, 3,* 85–87.

García de Madinabeitia, S., Sánchez Lorda, M. E., & Gil Ibarguchi, J. I. (2008). Simultaneous determination of major to ultra trace elements in geological samples by fusion-dissolution and inductively coupled plasma mass spectrometry techniques. *Analytica Chimica Acta, 625*(2), 117–130.

Gómez-Fernández, F., Castaño, M. A., Bauluz, B., & Ward, C. R. (2009). Optical microscope and SEM evaluation of roofing slate fissility and durability. *Materiales de Construcción, 59*(296), 91–104.

Gómez-Fernández, F., Vindel, E., Martín-Crespo, T., Sánchez, V., González Clavijo, E., & Matías, R. (2012). The Llamas de Cabrera gold district, a new discovery in the Variscan basement of northwest Spain: a fluid inclusion and stable isotope study. *Ore Geology Reviews, 46,* 68–82.

Gómez-Fernández, F., Cunningham, J. K., Caldevilla, P., Herrero-Hernández, A. & Beard, A. D. (2019). The source of Au and S of the orogenic gold deposits in the Llamas de Cabrera district

Journal : **Large 41513**	Article No : **147**	Pages : **23**	MS Code : **147**	Dispatch : **9-11-2020**

(Iberian Variscan Massif). *Life with Ore Deposits on Earth – 15th SGA Biennial Meeting 2019, Glasgow*, 2, 842–845

González Menéndez, L. & Suárez, O. (2004). Caracterización petrológica y geoquímica de los diques basálticos de Cadavedo (Valdés, Asturias). *Trabajos de Geología*, Univ. Oviedo, 24, 81–89

González-Menéndez, L., Gómez-Fernández, F., Cunningham, J. K., Caldevilla, P., Gallastegui, G., & Menéndez, S. (2019). Rifting, deformation, metamorphism, hydrothermalism and gold precipitation recorded in volcanic rocks (The Truchas Syncline, Variscan Belt, NW Spain). *Geophysical Research Abstracts, 21,* 9984–9994.

Grant, J. A. (1986). The isocon diagram: A simple solution to Gressens equation for metasomatic alteration. *Economic Geology, 81,* 1976–1982.

Grant, J. A. (2005). Isocon analysis: A brief review of the method and applications. *Physics and Chemistry of the Earth, 30,* 997–1004.

Groves, D. I., Golding, S. D., Rock, N. M. S., Barley, M. E., & McNaughton, N. J. (1988). Archean carbon reservoirs and their relevance to the fluid source for gold deposits. *Nature, 331,* 254–257.

Gromet, L. P., Dimek, R. F., Haskin, L. A., & Korotev, L. R. (1984). The "North American Shale Composite": Its compilation, major and trace element characteristics. *Geochimica et Cosmochimica Acta, 48,* 2469–2482.

Gutiérrez-Marco, J. C. (1997). *Tolmachovia babini* nov. sp., nuevo ribeirioide (Mollusca, Rostroconchia) del Ordovícico Medio de la Zona Centroibérica Española. *Geobios-Mémoire Spécial, 20,* 291–298.

Gutiérrez-Marco, J. C., Aramburu, C., Arbizu, M., Bernárdez, E., Hacar Rodríguez, M. P., Méndez-Bedia, I., et al. (1999). Revisión bioestratigráfica de las pizarras del Ordovícico Medio en el noroeste de España (Zonas Cantábrica, Asturoccidental-Leonesa y Centroibérica septentrional). *Acta Geológica Hispánica, 34*(1), 3–87.

Gutiérrez-Marco, J., Robardet, M., Rábano, I., Sarmiento, G. N., de San José, M., Herranz Araújo, P., & Pieren, A. (2002). Ordovician. In W. Gibbons & T. Moreno (Eds.), *The geology of Spain* (pp. 31–49). London: Geological Society of London.

Herron, M. (1988). Geochemical classification of Terrigenous sands and Shales from core or log data. *Journal of Sedimentary Research, 58*(5), 820–829.

Holland, T. J. B., & Powell, R. (1998). An internally consistent thermodynamic data set for phases of petrological interest. *Journal of Metamorphic Geology, 16*(3), 309–343.

Holland, T. J. B., Baker, J. M., & Powell, R. (1998). Mixing properties and activity-composition relationships of chlorites in the system MgO-FeO-Al_2O_3-SiO_2-H_2O. *European Journal of Mineralogy, 10,* 395–406.

Holland, T. J. B., & Powell, R. (2003). Activity-composition relations for phases in petrological calculations: an asymmetric multicomponent formulation. *Contributions to Mineralogy and Petrology, 145,* 492–501.

Jowett, E.C. (1991). Fitting iron and magnesium into the hydrothermal chlorite geothermometer. *In: GAC/MAC/SEG Joint Annual Meeting. Program and Abstracts*, 16, A62

Julivert, M. & Truyols, J. (1973). Memoria del mapa Geológico de España E. 1: 50.000 nº 14 (Gijón). Segunda Serie MAGNA, Primera edición. IGME, 48 pp.

Kesler, S. (2005). Ore forming fluids. *Elements, 1,* 13–18.

King, P.L. & White, A.R.J. (2003). Granites, volatile solubility and tracking the formation of magmatic fluids. In P. Blevin, M. Jones, & B. Chappel (Eds.), *Magmas to Mineralisation: The Ishihara Symposium, Geoscience Australia*, Record 2003/14, pp. 85–88.

Kleine, B. I., Skelton, A. D. L., Huet, B., & Pitcairn, I. K. (2014). Preservation of blueschists-facies minerals along a shear zone by coupled metasomatism and fast-flowing CO_2-bearing fluids. *Journal of Petrology, 55*(10), 1905–1939.

Kleine, B. I., Pitcairn, I. K., & Skelton, A. D. L. (2015). The mechanism of infiltration of metamorphic fluids recorded by hydration and carbonation of epidote-amphibolite facies metabasaltic sills in the SW Scottish Highlands. *American Mineralogist, 100,* 2702–2717.

Kleine, B. I., Pitcairn, I. K., & Skelton, A. D. L. (2016). Mineralogical controls on metamorphic fluid flow in metabasaltic sills from Islay, Scotland. *Lithos, 248–251,* 22–39.

Liu, J.-Q., Chen, L.-H., Zeng, G., Wang, X.-J., Zhong, Y., & Yu, X. (2016). Lithospheric thickness controlled compositional variations in potassic basalts of Northeast China by melt-rock interactions. *Geophysical Research Letters, 43,* 2582–2589.

Marcos, A., Pérez-Estaún, A., Pulgar, J. A., Bastida, F. & Vargas, I. (1980). Memoria explicativa del Mapa Geológico de España E: 1:50.000 nº 99 (Becerreá). 2ª serie MAGNA, Primera edición. IGME. 32 pp.

Matas, J. & Velando, F. (1982). Memoria explicativa del Mapa Geológico de España E: 1:50.000 nº 230 (Castrocontrigo). Información complementaria: Análisis Paleontológico. 2ª serie MAGNA, Primera edición. IGME. 27 pp.

Montero, P., Talavera, C., & Bea, F. (2017). Geochemical, isotopic, and zircon (U-Pb, O, Hf isotopes) evidence for the magmatic sources of the volcano-plutonic Ollo de Sapo Formation Central Iberia. *Geologica Acta, 15*(4), 245–260.

Orejana, D., Villaseca, C., Billström, K., & Paterson, B. A. (2008). Petrogenesis of Permian alkaline lamprophyres and diabases from the Spanish central system and their geodynamic context within Europe. *Contributions to Mineralogy and Petrology, 156,* 477–500.

Pearce, J. A. (1982). Trace element characteristics of lavas from destructive plate boundaries. In R. S. Thorpe (Ed.), *Andesites* (pp. 525–548). New York: Wiley.

Pérez-Estaún, A. (1974). Algunas precisiones sobre la sucesión ordovícica y silúrica de la región de Truchas. *Breviora Geológica Astúrica, 18,* 23–25.

Pérez-Estaún, A. (1978). Estratigrafía y estructura de la Rama S. de la Zona Asturoccidental-leonesa. *Memorias del Instituto Geológico y Minero de España, 92,* 1–151.

Phillips, G. N., & Evans, K. A. (2004). Role of CO_2 in the formation of gold deposits. *Nature, 429,* 860–863.

Phillips, G. N., & Powell, R. (2010). Formation of gold deposits: a metamorphic devolatilization model. *Journal of Metamorphic geology, 28,* 689–718.

Pitzer, K. S., & Sterner, S. M. (1994). Equations of state valid continuously from zero to extreme pressures for H_2O and CO_2. *Journal of Chemical Physics, 101*(4), 3111–3116.

Polechová, M. (2016). The bivalve fauna from the Fezouata Formation (Lower Ordovician) of Morocco and its significance for palaeobiogeography, palaeoecology and early diversification of bivalves. *Palaeogeography, Palaeoclimatology, Palaeoecology, 460,* 155–169.

Rollingson, H. (1993). *Using geochemical data: evaluation, presentation, interpretation*. Logman Group UK. 352 p.

Rodríguez Fernández, L. R., Pedrera, A., Pous, J., Ayala, C., González-Menéndez, L., Ibarra, P., et al. (2015). Crustal structure of the south-western termination of the Alpine Pyrenean-Cantabrian Orogen (NW Iberian Peninsula). *Tectonophysics, 663,* 322–338.

Rosenberg, P. E. (1967). Subsolidus relations in system $CaCO_3$-$MgCO_3$-$FeCO_3$. *American Journal of Science, 52*(5–6), 787–796.

Sparks, R.S.J. (2003). Dynamics of magma degassing. In: Oppenheimer, C., Pyle, D.M. & Barclay, J. (eds), Volcanic Degassing. *Geological Society of London Special Publication,* 213, pp. 5–22

Journal : **Large 41513**	Article No : **147**	Pages : **23**	MS Code : **147**	Dispatch : **9-11-2020**

Suárez, A., Barba, P., Heredia, N. & Rodríguez Fernández, L.R. (1994). *Mapa Geológico de la Provincia de León Escala 1:200.000*. Instituto Tecnológico Geominero de España (ITGE).

Suárez, O., Gallastegui, G., Cuesta, A., Corretgé, L.G. & Tarrío, L. (1993). Geoquímica de las rocas basálticas del Cabo Peñas (Zona Cantábrica). In *V Congreso de Geoquímica de España* (pp. 42–47). Serv. De. CEDEX. ISBN: 84–7790–156–2

Sun, S.S. & MacDonough, W.F. (1989). Chemical and isotopic systematics of oceanic basalts: implication for mantle composition and processes. In: Saunders A.D. & Norry, M.J. (eds), Magmatism in Ocean Basins . *Geological Society of London Special Publication*, 42, 313–345.

Taylor, S. R., & McLennan, S. H. (1985). *The Continental crust: Its composition and evolution* (p. 312). Oxford: Blackwell.

Truyols, J. & Julivert, M. (1976). La sucesión Paleozoica entre el Cabo Peñas y Antromero (Cordillera Cantábrica). *Trabajos de Geología*, Univ. Oviedo, 8, 5–30

Valverde-Vaquero, P. (1992). *Permo-Carboniferous magmatic activity in the Cantabrian Zone (NE Iberian Massif, NW Spain)*. Master of Science Boston College, 291 pp.

Valverde-Vaquero, P., & Dunning, G. R. (2000). New U-Pb ages for early Ordovician Magmatism in central Spain. *Journal of the Geological Society, 157,* 15–26.

Valverde-Vaquero, P., Hepburn, C. J., & MartínezGarcía, E. (2016). Geochemistry of the Upper Ordovician alkaline basalts of the Castro Fm: (Cantabrian Zone): break-up along the Ibero-Armorican margin of the Rheic Ocean? *Geo-Temas, 16*(2), 207–210.

Villa, L., Corretgé, L.G., Arias, D. & Suárez, O. (2004). Los depósitos volcanoclásticos sineruptivos del paleozoico inferior del área de lago-Fontarón (Lugo, España). *Trabajos de Geología*, Univ. Oviedo, 24, 185–205

Villar Alonso, P., Portero Urroz, G., González Cuadra, P., García Crespo, J., Nieto García, A.B., Rubio Pascual, F.J., Gómez-Fernández, F. & Giménez Benayas, S. (2019). Mapa Geológico Digital Continuo E. 1:50.000, Zona Centroibérica. Dominio Ollo de Sapo (Zona 1300). GEODE. Mapa Geológico Digital Continuo de España. Disponible en: https://info.igme.es/cartografíadigital/geologica/geodezona.aspx?id=Z1300

Villas, E., Gisbert, J., & Montesinos, R. (1989). Brachiopods from volcanoclastic Middle and Upper Ordovician of Asturias (Northern Spain). *Journal of Paleontology, 63*(5), 554–565.

Villaseca, C., Merino Martínez, E., Orejana, D., Andersen, T., & Belousova, E. (2016). Zircon Hf signatures from granitic orthogneisses of the Spanish Central System: Significance and sources of the Cambro-Ordovician magmatism in the Iberian Variscan Belt. *Gondwana Research, 34,* 60–83.

Yardley, B.W.D. & Bodnar, R.I. (2014). Fluids in the continental crust. *Geochemical Perspectives*, 3, n°1.

Ward, C. R., & Gómez-Fernández, F. (2003). Quantitative mineralogical analysis of Spanish roofing slates using the Rietveld method and X-ray powder diffraction data. *European Journal of Mineralogy, 15,* 1051–1062.

White, R. W., Powell, R., & Holland, T. J. B. (2007). Progress relating to calculation of partial melting equilibria for metapelites. *Journal of Metamorphic Geology, 25*(5), 511–527.

Zane, A., & Weiss, Z. (1998). A procedure for classifying rock-forming chlorites based on microprobe data. *Rendiconti Lincei Scienze Fisiche e Naturali Serie, 9*(1), 51–56.

Journal : **Large 41513**	Article No : **147**	Pages : **23**	MS Code : **147**	Dispatch : **9-11-2020**